



Interactions between precipitation, evapotranspiration and soil-moisture-based indices to characterize drought with high-resolution remote sensing and land-surface model data

Jaime Gaona^{1,2}, Pere Quintana-Seguí², María José Escorihuela³, Aaron Boone⁴, and María Carmen Llasat⁵

¹Instituto de Investigación en Agrobiotecnología, CIALE, Universidad de Salamanca, Villamayor, Salamanca, 37185, Spain

²Hydrology and climate change, Observatori de l'Ebre (Universitat Ramon Llull – CSIC), Roquetes, 43520, Catalonia, Spain

³IsardSAT, Parc Tecnològic – Barcelona Activa, Barcelona, 08042, Catalonia, Spain

⁴Groupe de Météorologie de Moyenne Echelle, MODélisation de l'Atmosphère Nuageuse et Analyse, GMME-MOANA, CNRM-GAME (URA CNRS & Météo-France), 42, Av. G. Coriolis, 31057, Toulouse CEDEX 1, France

⁵Department of Applied Physics, Faculty of Physics, University of Barcelona, Barcelona, 08028, Catalonia, Spain

Correspondence: Jaime Gaona (jaimegaona@usal.es)

Received: 21 February 2022 – Discussion started: 9 March 2022

Revised: 12 August 2022 – Accepted: 29 September 2022 – Published: 21 October 2022

Abstract. The Iberian Peninsula is prone to drought due to the high variability in the Mediterranean climate with severe consequences for drinking water supply, agriculture, hydropower and ecosystem functioning. Because of the complexity and relevance of droughts in this region, it is necessary to increase our understanding of the temporal interactions of precipitation, evapotranspiration and soil moisture that originate from drought within the Ebro basin, in northeastern Spain, as the study region. Remote sensing and land-surface models provide high-spatial-resolution and high-temporal-resolution data to characterize evapotranspiration and soil moisture anomalies in detail. The increasing availability of these datasets has the potential to overcome the lack of in situ observations of evapotranspiration and soil moisture. In this study, remote sensing data of evapotranspiration from MOD16A2 and soil moisture data from SMOS1km as well as SURFEX-ISBA land-surface model data are used to calculate the evapotranspiration deficit index (ETDI) and the soil moisture deficit index (SMDI) for the period 2010–2017. The study compares the remote sensing time series of the ETDI and SMDI with the ones estimated using the land-surface model SURFEX-ISBA, including the standardized precipitation index (SPI) computed at a weekly scale. The study focuses on the analysis of the time lags between the indices to identify the synchronicity and memory of the anomalies between precipitation, evapotranspiration

and soil moisture. Lag analysis results demonstrate the capabilities of the SPI, ETDI and SMDI drought indices computed at a weekly scale to give information about the mechanisms of drought propagation at distinct levels of the land–atmosphere system. Relevant feedback for both antecedent and subsequent conditions is identified, with a preeminent role of evapotranspiration in the link between rainfall and soil moisture. Both remote sensing and the land-surface model show capability to characterize drought events, with specific advantages and drawbacks of the remote sensing and land-surface model datasets. Results underline the value of analyzing drought with dedicated indices, preferably at a weekly scale, to better identify the quick self-intensifying and mitigating mechanisms governing drought, which are relevant for drought monitoring in semi-arid areas.

1 Introduction

Drought is a major natural hazard for societies in semi-arid climates (Van Loon, 2015) and demands increasing levels of adaptation and resilience measures to guarantee water supply (Watts et al., 2012), particularly in water-stressed environments. Rainfed agriculture (Tigkas and Tsakiris, 2015) and even the enduring natural vegetation are very exposed to drought, especially under climate change, which has long-

lasting implications for the local environment (Gudmundsson et al., 2014). Knowing that complex interactions take place in the land–atmosphere system under drought, the traditional meteorological or hydrologic approach may overlook drought-relevant interactions between evapotranspiration and soil moisture (Teuling et al., 2013).

To track drought status and to analyze the interactions of the land–atmosphere system, modern drought monitoring combines evapotranspiration, soil moisture and even vegetation anomalies in composite drought indices, such as the Objective Blends of Drought Indicators (OBDI) integrated in the U.S. Drought Monitor (USDM; Svoboda et al., 2002) or the Combined Drought Indicator (CDI) of the European Drought Observatory (Sepulcre-Canto et al., 2012). The use of this combined approach to monitoring drought is on an upward trend because even parsimonious composite drought indices like the probabilistic precipitation vegetation index (PPVI) (Monteleone et al., 2020) outperform the capabilities of common indices to characterize drought. One of the major advantages of composite indices is that they facilitate the characterization of drought from multiple perspectives (e.g., meteorological, hydrological or agricultural). Conversely, composite indices can be impractical to explore the mechanisms of drought, whose understanding may require focusing on key variables of the system. Unfortunately, evapotranspiration and soil moisture are still challenging to monitor compared to the meteorological, hydrological or vegetation variables currently regularly recorded. Despite the relevance of these two variables in the recurrence of drought and heat waves (Zampieri et al., 2009; Dasari et al., 2014), even at short timescales (Teuling, 2018), relatively few studies have evaluated their anomalies due to the limited availability of data of sufficient spatial and temporal resolution.

Well-known drought indices such as the standardized precipitation index (SPI) (McKee et al., 1993) and the Palmer drought severity index (PDSI) (Palmer, 1965), primarily defined on the monthly scale, can lack detail to identify short-term anomalies of temperature, wind or radiation-originating “flash droughts” (Otkin et al., 2013). Rainfed agriculture and natural vegetation are particularly sensitive to quickly evolving droughts in specific moments of the growing season (Saini and Westgate, 1999), which subsequently generate evapotranspiration and soil moisture anomalies of short- and long-term impact (Jiménez et al., 2011). Recently, there has been more interest in using drought indices with high temporal resolution for short-term drought monitoring, such as the SPI and other indices at the weekly scale (Otkin et al., 2015). Indices with this short-term timescale include the weekly-scale evapotranspiration deficit index (ETDI) and the soil moisture deficit index (SMDI) (Narasimhan and Srinivasan, 2005). The ETDI and SMDI are variable-specific, enabling full characterization of anomalies at specific levels of the land–atmosphere system. This is especially useful in the Mediterranean climates where drought originates from not only rainfall anomalies (Vicente-Serrano et al., 2004).

This study focuses on the Ebro basin, which is an important Mediterranean river basin of the Iberian Peninsula (IP). In view of the increase in the frequency of drought events (Sousa et al., 2011) and the number of consecutive dry spells (Turco and Llasat, 2011) identified in the area, we can expect consequences in the long-term environmental state and the balance between water availability and demands. Furthermore, being placed in a semi-arid climate where most of the rainfall evaporates (68 %, Table 15 of *Libro blanco del agua*; MMA, 2000), the Ebro basin represents an example of how important natural water demands are, particularly in the headwaters where reforestation decreases runoff (López-Moreno et al., 2014). Rainfed agriculture dominates the rest of the un-forested areas and represents the other big consumer of water in the basin. However, despite the relevance of rainfed agriculture, its analysis is often overshadowed by irrigation, the biggest anthropogenic demand in the basin (Hoerling et al., 2012). Due to the importance of these water demands and others such as hydropower and energy, the Ebro Hydrographic Confederation operates a dense hydrologic monitoring network, but the lack of dedicated soil moisture and evapotranspiration monitoring jeopardizes drought characterization (Seneviratne et al., 2010). Fortunately, the increasing availability of remote sensing (RS) products enables distributed, precise and frequent monitoring of these coarsely observed variables (Martínez-Fernández et al., 2016).

Space agencies have released multiple RS products in the last decade facilitating the distributed analysis of drought (AghaKouchak et al., 2015). Optical spectrometry of the atmospheric (rainfall, temperature, water vapor) and surface (vegetation reflectance) variables has often been the basis for distributed characterization of drought indicators. Surface vegetation indices such as the widespread normalized difference vegetation index (NDVI; Liu and Kogan, 1996) pioneered the application of RS data to assess the impacts of drought, but thereafter the increasing availability of RS data for multiple meteorological variables has increased their usage in drought indices (West et al., 2019). Currently, common indices like the SPI can rely on RS data (Sahoo et al., 2015) because integrating the increasing resolution of RS data into drought indicators enables short-term drought monitoring at least at the weekly scale (USDM – Svoboda et al., 2002; CDI – Sepulcre-Canto et al., 2012; Monteleone et al., 2020). However, unlike precipitation, temperature, and other directly observable and densely monitored meteorological variables, the measurement of evapotranspiration and soil moisture on the ground is still challenging and often costly or impractical at sufficient spatial resolution. Overcoming this gap is possible now thanks to the increasing availability of RS-based evapotranspiration databases such as the global dataset included in GLEAM (Miralles et al., 2011; Martens et al., 2017) or the soil moisture global database CCI (Dorigo et al., 2017). Despite the coarse spatial resolution of these global datasets, the recent developments in

RS processing and downscaling improve their applicability at regional spatial scales and short timescales (Wagner et al., 2007). Aiming to gain insight into drought mechanisms, the availability of high-resolution datasets focused on such relevant variables of the land–atmosphere facilitates the use of single-variable drought indices such as the SPI, ETDI and SMDI, which is advantageous to analyze the interactions between variables during droughts.

On this basis, there are soil moisture datasets of increasingly high resolution available from a combination of passive microwave sensors such as those from SMOS and Soil Moisture Active Passive (SMAP) missions (Kerr et al., 2010, and Entekhabi et al., 2010, respectively) and active microwave sensors such as ASCAT or Sentinel-1 (Bartalis et al., 2007, and Hornacek et al., 2012, respectively). This is the case of the high-resolution soil moisture product SMOS1km (Merlin et al., 2013; Molero et al., 2016; Escorihuela and Quintana-Seguí, 2016; Escorihuela et al., 2018), which has been tested in the area and has been shown to outperform ASCAT and AMSR-E due to its lack of roughness and vegetation effects. SMAP and Sentinel-1 options are of similar resolution to SMOS1km and accurate in the study area (Dari et al., 2021), but they are of much shorter series length and are consequently not selected. Similarly, high-resolution RS evapotranspiration products such as MOD16A2 (Mu et al., 2013) used in this study are currently available. Therefore, it is worth exploring the capabilities and limitations of high-resolution RS evapotranspiration data for drought monitoring at the regional scale. High-resolution RS data are most suitable for analysis at the basin scale where the resolution of alternative reanalysis or modeled datasets such as ERA5-Land (Muñoz-Sabater et al., 2021), LISFLOOD (Van Der Knijff et al., 2008) or GLEAM v3 (Miralles et al., 2011; Martens et al., 2017) lack detail. To date, relatively few works have used high-resolution satellite data for drought analysis in the IP (Vicente-Serrano, 2006; Scaini et al., 2015; Martínez-Fernández et al., 2016; Sánchez et al., 2016; Ribeiro et al., 2019), especially at the spatial and temporal resolution of this study (Pablos et al., 2017).

Another source of high-temporal-resolution and high-spatial-resolution data is land-surface models (LSMs). Used in atmospheric models to simulate the interactions between soil, vegetation and the atmosphere, LSMs represent a suitable alternative to RS to evaluate the surface water and energy balances at regional to local scales. The development of LSMs was initiated with one-layer models such as TOPUP (Schultz et al., 1998) or PROMET (Mausser and Schadlich, 1998). Avissar and Pielke (1989) inaugurated the mosaic approach, applying just one-layer models to the different fractions of land-use type. One of the mosaic models able to distinguish between soil evaporation and transpiration is the Météo-France-developed model SURFEX (Masson et al., 2013), which, fed by the atmospheric analysis SAFRAN (Durand et al., 1999), uses the ISBA scheme for natural surfaces (Noilhan and Mahfouf, 1996). SURFEX has been im-

proved to study the continental water cycle in applications such as SIM and SIM2 (Habets et al., 2008; Le Moigne et al., 2020), often in combination with the hydrologic model MODCOU (Ledoux et al., 1989). The modeling chain called SASER (SAFRAN–SURFEX–Eaudyssée–RAPID) used in this study has been applied to Spain before (Barella-Ortiz and Quintana-Seguí, 2019; Quintana-Seguí et al., 2020). This LSM provides the precipitation required for the SPI and the evapotranspiration and soil moisture necessary to generate LSM-based ETDI and SMDI series comparable to the ones generated using RS data. Despite the limitations of this LSM when applied as an offline model, it has been validated and shown to provide useful evaluations of water resources in the study area (Escorihuela and Quintana-Seguí, 2016; Barella-Ortiz and Quintana-Seguí, 2019) and nearby Portugal and France (Nogueira et al., 2020; Le Moigne et al., 2020).

This study aims at evaluating the suitability of high-resolution RS (SMOS1km and MOD16A2) and LSM (SURFEX-ISBA) data for generating rainfall (SPI), soil moisture (SMDI) and evapotranspiration (ETDI) drought (single-variable) indices to better understand the mechanisms behind the temporal evolution of drought in semi-arid climates. The comparison of RS and LSM data results is a main aim of the study to detect the factors impacting drought indices based on RS and LSM data. The study further evaluates the advantage of the barely explored weekly temporal scale to capture the short-term anomalies of evaporation and soil moisture decisive for drought in semi-arid areas. The study has an agricultural scope focused on drought in rainfed environments given its importance to land–atmosphere feedbacks (Herrera-Estrada et al., 2017) and regional socioeconomic sustainability.

2 Study area

The study area is the Ebro basin, located in the northeast of the Iberian Peninsula (IP). Placed in between Atlantic and Mediterranean climatic influences, the vast area (85 534 km²) of the basin (Fig. 1a) has a complex topography (Fig. 1c) which defines a wide range of climatic conditions (Fig. 1d) of distinct spatial and temporal patterns of precipitation, evapotranspiration and soil moisture. The northern border has humid cool climates typical of the Atlantic-exposed Cantabrian coastline, while the southeastern border enjoys a warm Mediterranean climate. The southwestern and northeastern borders are dominated by the Iberian and Pyrenees mountains which together with the Cantabrian and Mediterranean ranges restrict the oceanic influence on the central part of the basin. Soil types (e.g., gypsum, limestones) intensify the aridity of certain areas of the basin (Fig. 1b). The combination of semi-arid climatic conditions and unfavorable soil types to vegetation development determines extreme regimes of rainfall, soil moisture and evapotranspiration, prone to drought. The basin is densely populated and

supplies a wide range of water demands, especially for agriculture and energy. The vast network of irrigated areas, located mostly in the arid central depression, is vulnerable to hydrological drought risks.

3 Data

3.1 Land-surface model data

SURFEX, the land-surface modeling platform originally developed and currently maintained by Météo-France (Masson et al., 2013; Le Moigne et al., 2020), has been chosen to perform the LSM simulation used in this study. Simulations for the IP and Balearic Islands developed within the HUMID project have 5×5 km spatial resolution and use the forcing provided by the Iberian application (Quintana-Seguí et al., 2008, 2016, 2017) of the SAFRAN meteorological analysis system (Durand et al., 1999). This is a modeling chain whose offline mode operates using the atmospheric forcing of SAFRAN to feed the LSM SURFEX-ISBA and simulate even the hydrology with Eaudyssée–RAPID (David et al., 2011).

ISBA (Noilhan and Mahouf, 1996) is the SURFEX module in charge of simulating natural surfaces. There are different versions of ISBA. In this study, we have used the diffusion version (ISBA-DIF; Boone, 1999; Decharme et al., 2011), which performs better in the study area than the simpler three-layer force restore version (Quintana-Seguí et al., 2020). In this version of ISBA, the leaf area index (LAI) has a prescribed annual cycle (constant every year), which may limit the ability of the model to reproduce the long-term effects of drought on vegetation. The model simulates the soil column, but it is unable to simulate groundwater, which despite its impact on soil moisture memory, is not very relevant in the Ebro basin. SURFEX-ISBA requires additional physiographic information that is incorporated from the ECOCLIMAP-II land cover database (Faroux et al., 2013), which includes topographic, soil and land cover information at high resolution.

The available SAFRAN forcing data allow us to simulate the period 1979–2017, but the period used for this study is restricted by the relatively short length of the RS SMOS data coverage (2010–present) compared to the model. To ensure the comparability of RS-based and LSM-based drought indices, the study period is 2010–2017, for which both RS and LSM data are available. To ensure that the RS soil moisture and the LSM soil moisture are comparable, we have averaged the first three soil layers of the model according to their discretization in the first 5 cm of the soil (1, 3 and 10 cm of depth, respectively). The simulation is performed using a regular 5×5 km resolution grid based on a custom Lambert conformal conic projection.

3.2 Remote sensing data

3.2.1 Evapotranspiration

To evaluate evapotranspiration, barely measured on the ground and not directly measurable from space, we adopt a product based on multiple evaporation-related variables observed by MODIS (Moderate Resolution Imaging Spectroradiometer on NASA's Terra satellite): the MOD16A2 dataset. This is a level-4 product providing 8 d evapotranspiration (ET) and potential evapotranspiration (PET) based on daily meteorological forcing and 8 d RS data of vegetation dynamics from MODIS (Mu et al., 2013). The datasets of MOD16A2 are published in a sinusoidal projection at a resolution of 500 m (Running et al., 2017). In this study, we have reprojected and interpolated all RS products to the same 5×5 km grid that the LSM simulations use. After the re-gridding step, the temporal step of the datasets is rearranged from the original 8 d accumulation period to a 7 d accumulation period, which is more suitable for weekly analysis. Values are linearly weighted depending on their contribution to each week for the 52 weeks of a year. We also calculate the monthly means of the evapotranspiration product to evaluate the impact of the time resolution on drought recognition. The formatting of MOD16A2 datasets requires the evaluation of the quality control flags (ET_QC), given that areas of the Pyrenees show missing data. Only the classes classified as good and optimal in the ET_QC flags are accepted as data for our study.

3.2.2 Surface soil moisture

Because of the relatively few years of data currently available from the Soil Moisture Active Passive (SMAP) mission (Entekhabi et al., 2010), the study adopts SMOS data (Kerr et al., 2010), in particular, the high-resolution SMOS1km dataset (Merlin et al., 2013). This dataset downscales the original coarse-resolution SMOS data using the Disaggregation based on Physical And Theoretical scale Change (DISPATCH) algorithm (Merlin et al., 2012) and the C4DIS algorithm (Molero et al., 2016). The algorithm enables the downscaling of the 40 km resolution of the SMOS soil moisture data available from 2010 into 1 km resolution using two products at 1 km resolution from MODIS, the NDVI and land surface temperature (LST), and an elevation map at the same resolution. Precisely because the scale of interest to study relevant interactions to droughts is the weekly scale, the data are primarily used on a weekly scale. The spatial scale of interest for the study is that of a regular 5×5 km resolution grid, which takes advantage of the high resolution of SMOS1km. The 2010–2017 dataset presents frequent gaps in the mountainous areas of the Pyrenees. In order to fill the gaps, we apply temporal interpolation pixel by pixel considering a maximum period for temporal interpolation of 2 weeks. These

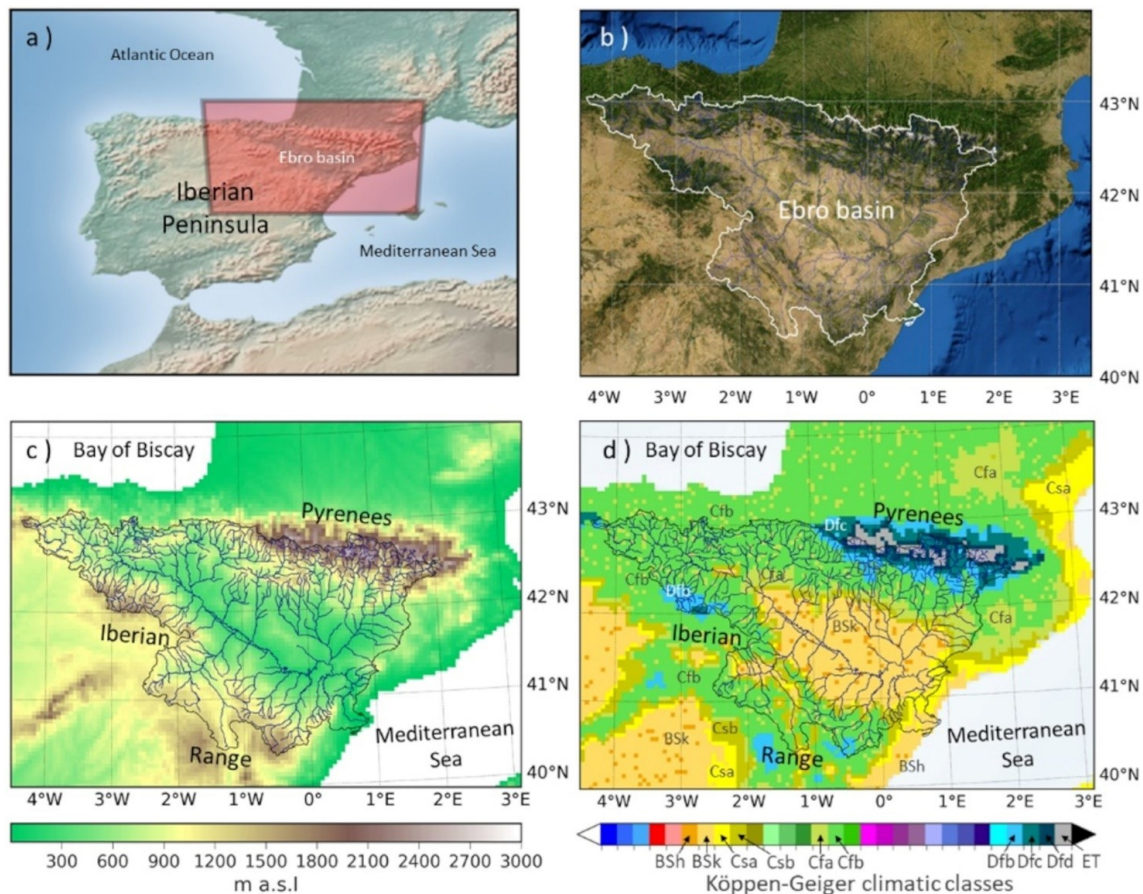


Figure 1. (a) Ebro basin location in the Iberian Peninsula (OSM OpenTopoMap). (b) Land cover of the basin depicting a contrasting basin between the forested areas of the mountains and the steppes of the central depression (© Esri satellite online maps, World Imagery, 2022). (c) Altitudinal range of the basin (IGN ES/FR MDT25, CC-BY 4.0). (d) Climatic classes present in the basin according to the climatic classification of Köppen–Geiger (data from Beck et al., 2018).

data are also spatially aggregated and reprojected onto the same grid as the LSM.

4 Methods

4.1 Drought indices

Drought indices allow quantifying several aspects of drought, like the magnitude and duration, and may also focus on particular variables depending on the scope of interest (i.e., precipitation, soil moisture, aridity, etc.). In view of the convenience to combine several single-variable indicators to describe most of the drought mechanisms and our focus on rainfed environments, we adopt the use of the standardized precipitation index (SPI) (McKee et al., 1993), the evapotranspiration deficit index (ETDI) and the soil moisture deficit index (SMDI) (Narasimhan and Srinivasan, 2005). Using these three indices, the study aims to investigate the interaction between the two main water fluxes (rainfall and evapotranspiration) and the main storage (soil moisture) involved in

the water balance of the land–atmosphere system. The aggregation periods of the SPI inform us about the different responding times of rainfall, soil moisture, streamflow and groundwater anomalies. By evaluating the evolution of these indices along with their interactions, this study aims to characterize drought mechanisms in the Ebro basin. In this study, the indices have been computed using gridded datasets, thus generating a time series for each grid point.

4.1.1 SPI

The standardized precipitation index (SPI) (McKee et al., 1993) is an index of precipitation anomalies, which is calculated by transforming the accumulated precipitation from its original distribution (usually gamma or Pearson type III) to the normal distribution with zero mean and unit standard deviation. As a result, we obtain a time series that shows, for each time step, the departure from the expected value in terms of standard deviations. The calculation of the index is usually made based on monthly time series of rainfall, ag-

gregated over multiple accumulation periods, typically at 3, 6 and 12 months. However, the SPI can also be calculated on a weekly basis, provided that the accumulation periods are at least 4 weeks (1 month). In this way, this study uses the notation SPI_m-i to denote the SPI at a monthly scale with an accumulation period of i months and SPI_w-i to denote the weekly SPI with an accumulation period of i weeks. Using SAFRAN data, we adopt the non-parametric methodology proposed by Farahmand and Aghakouchak (2015) to calculate the SPI on a monthly and weekly basis using the multi-month accumulation of 1, 3, 6 and 12 months suitable for rainfall, soil moisture, streamflow and groundwater evaluation.

4.1.2 ETDI

The second index incorporated into the analysis is the evapotranspiration deficit index (ETDI) defined by Narasimhan and Srinivasan (2005). The first step for calculating this index implies defining the water stress (WS) ratio for each week, which is the difference between potential evapotranspiration (PET) and actual evapotranspiration (AET) divided by PET. Then the water stress anomaly (WSA) is computed as follows:

$$WSA_{i,j} = \frac{MWS_j - WS_{i,j}}{MWS_j - \min WS_j} \times 100 \text{ if } WS_{i,j} \leq MWS_j,$$

$$WSA_{i,j} = \frac{MWS_j - WS_{i,j}}{\max WS_j - MWS_j} \times 100 \text{ if } WS_{i,j} > MWS_j, \quad (1)$$

where j denotes the week of the year ($1 \leftarrow j \leftarrow 52$) and i denotes the year. $WS_{i,j}$ is the water stress of the week j of the year i . MWS_j is the median WS for the week j of the year; $\min WS_j$ corresponds to the minimum and $\max WS_j$ to the maximum. This process removes the seasonality of the time series. WSA ranges from -100 (maximum water stress) to 100 (minimum water stress). The WSA accumulates over time to define the ETDI as in the following equation:

$$ETDI_j = 0.5ETDI_{j-1} + \frac{WSA_j}{50}. \quad (2)$$

To define a range between -4 and 4 for the index, the ETDI of value -4 must correspond to a WSA of value -100 and the ETDI of value 4 to a WSA of value 100 . This range adjustment determines the coefficients 0.5 and the divisor 50 of Eq. (2). In this way, the ETDI becomes a non-seasonal index suitable for comparing time series of diverse climatic characteristics. Monthly values of the ETDI are calculated by computing the average of the weekly values of the corresponding month. In this study, we calculate the ETDI using potential and actual evapotranspiration provided by MOD16A2. We have also calculated it using the SURFEX-ISBA-simulated AET and PET. By default, SURFEX-ISBA does not calculate potential evapotranspiration. In order to do so, we have modified the source code to set soil moisture permanently

at field capacity and have run a simulation with this modification. The resulting evapotranspiration corresponds to the potential one.

4.1.3 SMDI

The third index incorporated into the analysis is the soil moisture deficit index (SMDI) also defined by Narasimhan and Srinivasan (2005). The sequence to calculate this index follows the same procedure as the ETDI. We first calculate a weekly soil moisture deficit (SD) as follows:

$$SD_{i,j} = \frac{SW_{i,j} - MSW_j}{MSW_j - \min SW_j} \times 100 \text{ if } SW_{i,j} \leq MSW_j,$$

$$SD_{i,j} = \frac{SW_{i,j} - MSW_j}{\max SW_j - MSW_j} \times 100 \text{ if } SW_{i,j} > MSW_j. \quad (3)$$

Then, the time series of the SMDI is generated accumulating the SD:

$$SMDI_j = 0.5SMDI_{j-1} + \frac{SD_j}{50}. \quad (4)$$

The SMDI also ranges between -4 and 4 , corresponding to extremely dry and very wet soil moisture conditions, respectively. The SMDI, similarly to the ETDI, becomes a non-seasonal index able to compare time series of diverse climatic characteristics at different soil depths. In this study, we have calculated the SMDI using SMOS1km surface soil moisture data and SURFEX-ISBA-simulated surface soil moisture data. In the case of SURFEX-ISBA, we have calculated the weighted averages of the first two layers of the soil, which correspond to the first 5 cm of the soil.

4.1.4 Temporal consistency of drought indices calculated based on relatively short RS and LSM data series

Given the relatively short availability of data for the calculation of ETDI and SMDI series, which depend on the maximum, minimum and median values of the available series, we conducted a sensitivity analysis of the indices in reference to the length of the series and the subset of spatial data. Results shown in Table S1 illustrate the relatively low impact of the length of the series thanks to the high spatial resolution of the dataset. The shortening of the series by half or a quarter barely alters the ETDI series compared to the case of using the full temporal length. The subset of the dataset to a fraction of its spatial resolution increasingly impacts the robustness of ETDI and SMDI series. Therefore, the high-resolution spatial and temporal datasets such as the RS and LSM used for this study support the consistency of drought indices even when data availability remains under a decade long.

4.2 Analysis of interaction between the indices

4.2.1 Correlation between the indices

To evaluate the similarity between the series of the drought indices (SPI, ETDI and SMDI), we use a variant of the procedure applied by Barella-Ortiz and Quintana-Seguí (2019) and Quintana-Seguí et al. (2020), based on Barker et al. (2016). The method consists of computing the r Pearson correlation between each pair of series of these three drought indices (e.g., SPIw- i and ETDIw and SMDIw), where i is the accumulation period, which varies from 4 weeks (1 month) to 52 weeks (1 year). For this evaluation and the following lag analysis, we adopt the r Pearson coefficient because the time it consumes to process our RS and LSM datasets is an order of magnitude lower (e.g., weeks) than the time required using r Spearman (e.g., months). To further support the use of r Pearson despite the concerns about the non-normality of SMDI and ETDI distributions, we conducted a similarity test of the series of lags between indices obtained with r Pearson and r Spearman. Similarity tests indicate r Pearson and r Spearman correlate generally over $r = 0.9$ for RS data and at a moderately lower level for LSM data, while they do not differ significantly in the timing characteristics of the series (Fig. S1 in the Supplement). Therefore, we can consider r Pearson suitable and sufficiently accurate for the approach and focus of the study.

4.2.2 Temporal lag analysis of the indices

Following the correlation analysis between the series, we perform a lag analysis of the correlation of the pairs of drought indices at a weekly scale, introducing lags from -104 weeks to $+104$ weeks. We compare ETDIw and SMDIw with SPIw- i (being the period of accumulation for SPIw- i , where i is 4, 13, 26 and 52 weeks, equivalent to SPIm-1, SPIm-3, SPIm-6 and SPIm-12), as well as ETDIw with SMDIw. The purpose of this analysis is to diagnose the reciprocity and memory in the interaction between rainfall and evapotranspiration and between rainfall and surface soil moisture. The relative abundance of positive over negative lags (and vice versa) provides information about the asymmetry of the interaction between the indices (precedence and delay). Negative lags refer to leading times of ETDIw and SMDIw with respect to SPIw- i (e.g., lag -104 , left side of the time bar), while positive ones (e.g., lag $+104$) represent lag times when SPIw- i precedes ETDIw and SMDIw (e.g., lag $+104$, right side of the time bar). The number of consecutive weeks of positive or negative lags of SPIw- i can inform us about the memory of the interactions. For each time lag, the percentage of the basin affected by non-significant/significant correlations is indicated (grey/colored scales of bars in Figs. 3–7). Positive/negative correlations indicate a direct/indirect relationship (red/blue bars in Figs. 3–7).

5 Results

5.1 Correlation between indices: monthly scale in comparison to the weekly scale

The first two aims of the study are to evaluate the suitability of the SPI, ETDI and SMDI to characterize the main anomalies in water exchanges of the land–atmosphere system and to evaluate the suitability of adopting the weekly scale for the analysis of drought indices compared to the use of the monthly scale. Regarding the first, results shown in Fig. 2 indicate a general agreement of the SPI, ETDI and SMDI (computed at either a monthly or a weekly scale) on the major events of dry and wet anomalies of the period 2010–2017. The dry period of 2011–2012 and the wet period from the end of 2012 to 2015 were properly depicted. However, we identified differences, especially in the case of the SMDI. This index tends to show a generally lower variability than other indices when calculated with the LSM. RS results of the SMDI differ from the other indices during the start of 2010 due to the uncertainties during the test period of the SMOS mission. The left column of Fig. 2 shows the monthly SPIm- i and the monthly averaged ETDIm and SMDIm. Correlations between the SPI and the ETDI and SMDI are calculated on the monthly scale (Table 1, top row) and on the weekly scale (bottom row) for both RS and LSM data (where $i = 4, 13, 26$ and 52 weeks of aggregation, equivalent to 1, 3, 6 and 12 months). We test the significance of the correlations (p value < 0.05) between indices for two subsets: the entire period (2010–2017) and a subset of dry periods (i.e., when SPI < 0 , ETDI < 0 , SMDI < 0). Then, we compare the observed (RS) and simulated (LSM) estimates of the indices to explore differences between data sources. RS and LSM ETDIm and SMDIm indices are moderately correlated (barely over 0.5, significant). Table 1 reports a value of $r = 0.58$ (significant) between ETDIm RS and SMDIm RS, which is significantly higher than the $r = 0.32$ between the ETDIm LSM and SMDIm LSM. In general, despite the resemblance of RS and LSM series of the ETDI and SMDI shown in Fig. 2, these two series differ. There is a higher agreement between the RS and the LSM estimates of ETDIm ($r = 0.77$, significant) than between the RS and LSM ones of SMDIm ($r = 0.27$).

Table 1 also reveals differences in the moderate correlation of SPIm- i with the ETDI and the SMDI of different temporal aggregations ($i = 1, 3, 6, 12$ months of SPIm- i accumulation) as well as between their RS and LSM versions. Correlation between SPIm and ETDIm RS increases with the aggregation period of SPIm ($r = 0.39, 0.62, 0.72$ and 0.81 for SPIm-1, SPIm-3, SPIm-6 and SPIm-12, respectively) while correlations of SPIm with the ETDI LSM peak at SPIm-3 ($r = 0.8$) and remain high for SPIm-6 ($r = 0.78$) and SPIm-12 ($r = 0.71$). The correlations between SPIm- i and SMDI RS show moderate correlation ranging from SPIm-1 ($r = 0.42$) to the maximum value of SPIm-12 ($r = 0.63$). The SMDIm LSM exhibits a decreasing correlation pattern

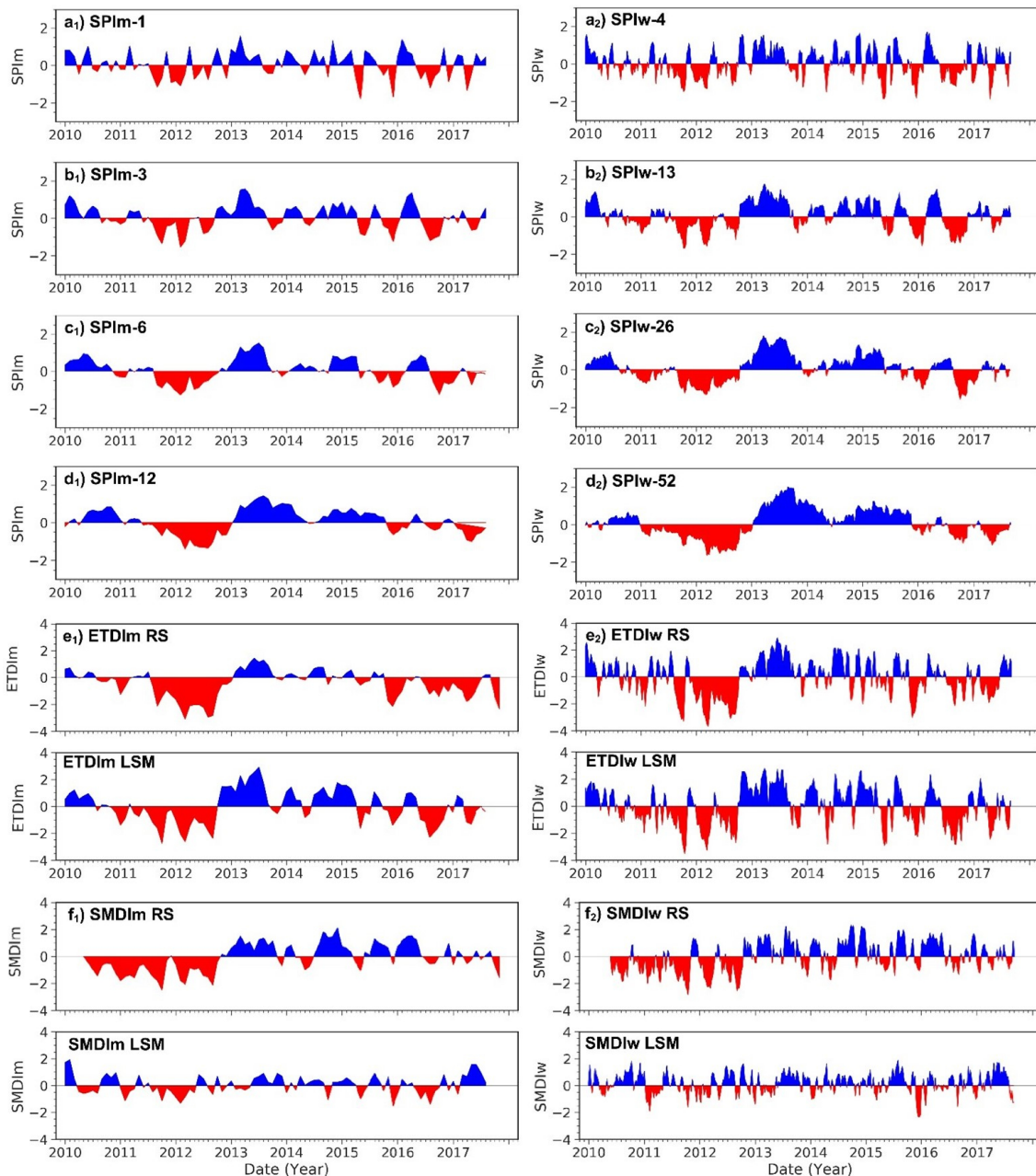


Figure 2. Time series of the SPI, ETDI and SMDI at the monthly scale (left column of subplots identified with sub-index 1) and weekly scale (right column of subplots identified with sub-index 2). Panels (a) to (d) correspond to SPI_m-1, SPI_m-3, SPI_m-6 and SPI_m-12; panels (e) and (f) display the temporal evolution of the ETDI and SMDI. These ones show two rows corresponding to the series based on RS and LSM data. Red/blue color represents dry/wet periods. Periods of drought occur when SPI < 0, ETDI > 0 and SMDI < 0.

with the increasing aggregation of SPI_m from SPI_m-3 to SPI_m-12 ($r = 0.45, 0.31, 0.3$ and 0.24 for SPI_m-1, SPI_m-3, SPI_m-6 and SPI_m-12, respectively). Remarkably, correlations of the LSM SPI_m–SMDIm are lower than their RS pairs, which suggests data uncertainties in RS and the LSM, as reported by Barella-Ortiz and Quintana-Seguí (2019) and by Quintana-Seguí et al. (2020).

The monthly correlation analysis is additionally conducted for the subsets of dry periods (those with negative signs of SPI_m, ETDIm and SMDIm). Using the dry subset instead of the entire period primarily decreases all correlations. Compared to the correlations of the entire period, the RS ETDIm–SMDIm values decrease a little while the LSM ones increase a little. Also the SPI_m-*i*–ETDIm and the SPI_m-*i*–SMDIm correlations decline noticeably. Despite the loss of corre-

Table 1. Matrices of significant (in bold) correlation coefficients considering a p values of = 0.05 for pairs of indices at the monthly and weekly scale for the period 2010–2017 of the SPI, ETDI and SMDI series and the corresponding dry-period subsets. Higher correlation values show a more intense red color. Since the correlations of interest refer to comparing the same type of data source for different indices, dark grey cells identify unsuitable combinations for the analysis such as comparing RS results from one index with LSM results from another index.

		2010-2017 - monthly scale				2010-2017 - monthly scale - dry periods			
		ETDI		SMDI		ETDI		SMDI	
		RS	LSM	RS	LSM	RS	LSM	RS	LSM
ETDI	RS		0.77	0.58			0.60	0.50	
	LSM	0.77			0.32	0.60			0.43
SMDI	RS	0.58				0.50			0.13
	LSM		0.32	0.27			0.43	0.13	
SPI	SPI _{m-1}	0.39	0.51	0.42	0.45	0.23	0.37	0.52	0.59
	SPI _{m-3}	0.62	0.80	0.61	0.41	0.42	0.67	0.41	0.32
	SPI _{m-6}	0.72	0.78	0.58	0.30	0.45	0.39	0.19	0.17
	SPI _{m-12}	0.81	0.71	0.63	0.24	0.75	0.53	0.40	0.22
		2010-2017 - weekly scale				2010-2017 - weekly scale - dry periods			
		ETDI		SMDI		ETDI		SMDI	
		RS	LSM	RS	LSM	RS	LSM	RS	LSM
ETDI	RS		0.55	0.50			0.34	0.46	
	LSM	0.55			0.21	0.34			0.18
SMDI	RS	0.50			0.19	0.46			0.12
	LSM		0.21	0.19			0.18	0.12	
SPI	SPI _{w-4}	0.57	0.68	0.57	0.33	0.30	0.49	0.57	0.25
	SPI _{w-13}	0.63	0.74	0.51	0.21	0.32	0.47	0.36	0.29
	SPI _{w-26}	0.57	0.60	0.40	0.16	0.21	0.30	0.40	0.02
	SPI _{w-52}	0.48	0.45	0.43	0.15	0.31	0.16	0.39	-0.03

* Dry periods considered when SPI<0, ETDI<0 and SMDI<0.

lation and significance with the dry subset, the increase in the period of aggregation causes an increase in correlations, equal to the case of the entire period series.

Figure 2 provides an overview of the effect of adopting the weekly scale (right column) instead of the monthly scale (left column). The weekly scale substantially improves the temporal resolution of the plots. Subplots of SPI- i (a–d), the ETDI (e) and the SMDI (f) show how the weekly scale accurately reproduces the magnitude, tendency and duration of the monthly-scale anomalies, while the increase in temporal resolution additionally captures quick changes. Graphically, we noticed that the aggregation period applied to the SPI counteracts the gain in the resolution of the weekly scale, which often prevents users from adopting the weekly scale instead of the monthly scale. Conversely, Fig. 2e2 and f2 illustrate the strong increase in the resolution of the ETDI and SMDI resolution on the weekly scale.

The right columns of Table 1 indicate the correlations between indices on a weekly scale compared to those on a monthly scale (the “w” sub-index of ETDI_w, SMDI_w and SPI_w denotes the weekly scale). There is an overall decrease in correlations at the weekly scale compared to the monthly scale, accentuated by the increasing period of aggregation (from SPI_{w-3} to SPI_{w-12}). Correlations increase compared to the monthly scale at the lowest period of aggregation

of SPI_{w- i} , especially for SPI_{w-1}–ETDI_w (from $r = 0.39$ to $r = 0.57$) compared to SPI_{w-1}–SMDI_w (from $r = 0.51$ to $r = 0.68$). For both RS and LSM data, the weekly scale lowers the correlation values of SPI_{w- i} with SMDI_w more than those with ETDI_w. Within the dry-period subset, all the correlations decrease too. The weekly scale lowers correlations due to the increase in variability in the weekly time series compared to the monthly ones but enables capturing the increasing complexity of interactions at shorter timescales. Therefore, since quick shifts (Fig. 2e1 and f1) are of great interest for drought analysis, we consider the weekly scale the most convenient for the lag analysis of the next section. This decision benefits comparing drought indices at their highest temporal definition, which for the ETDI and SMDI is natively the weekly scale and for the SPI can be easily adopted.

5.2 Temporal lag analysis

The analysis of correlations between pairs of temporally lagged time series of drought indices provides valuable insights into the interactions between indices (e.g., in terms of reciprocity) as indicators of synchronicity of one variable with respect to the other. The analysis addresses the characterization of the interactions between rainfall, evapotranspiration and soil moisture while also aiming to examine

whether the land–atmosphere exchange of semi-arid areas under drought events is a quickly evolving or rather inertial system. Plots of the fraction of the area affected by each correlation level (from -1 to 1 in steps of $r = 0.2$) for each lag period are shown in Figs. 3–7. It is anticipated that the three evaluated indices agree the most in a narrow range around lag = 0 (no lag) and that their correlation fades away progressively for the increasing lag periods beyond the scale of the propagation of drought. Figures 3 to 6 in which SPIw- i interacts with the ETDI and SMDI illustrate the range of aggregation periods of SPIw (i.e., from 4 weeks of aggregation SPIw-4 to 52 weeks SPIw-52) along which the interpretation of the interactions between drought indices becomes most altered. The range of aggregation periods aims to open discussion about the optimal timescale to analyze the interacting drought processes. In general, the upper two subplots of Figs. 3 to 6 identify the admissible aggregation periods to interpret the clusters of interaction (SPIw-4 and SPIw-13, equivalent to SPI-1 and SPI-3 on a monthly scale), while the bottom two subplots (SPIw-26 and SPIw-52, equivalent to SPI-6 and SPI-12 at the monthly scale) depict the increasingly merged clusters of interaction due to excessively long aggregation periods of the SPI.

5.2.1 Lag analysis SPI–ETDI

RS

The lag analysis of SPIw–ETDIw and SPIw–SMDIw shown in Figs. 3–6 aims at diagnosing the reciprocity, synchronicity and memory in the interaction between rainfall and evapotranspiration and between rainfall and surface soil moisture. Each subplot of Figs. 3–6 shows the correlation between the ETDIw and SMDIw indices with SPIw- i calculated for different aggregation periods (i) at the weekly scale: SPIw-4, SPIw-13, SPIw-26 and SPIw-52. Negative lags refer to leading times of ETDIw and SMDIw with respect to SPIw- i (e.g., lag -104 , left side of the time bar) while positive ones (e.g., lag $+104$) represent lag times when SPIw- i precedes ETDIw and SMDIw (e.g., lag $+104$, right side of the time bar).

In the case of the ETDIw–SPIw- i analysis based on the RS data, there is a remarkable cluster of positive correlations in the short term (indicated with the tag ST₁ (short-term) over the subplots of Fig. 3). This ST₁ cluster shows relevant fractions of the basin affected by significant moderate (0.4 – 0.6) values of correlation, particularly in the first weeks of the positive range of lags (from lag 0 to $+4$) (Fig. 3). The cluster lasts more with the increasing period of aggregation (Fig. 3a to d), eventually becoming merged with the mid-term clusters. In view of subplots Fig. 3a to d, the ST₁ cluster extends from lag -13 to 4 in the case of SPIw-4; from lag -13 to $+13$ in the case of SPIw-13; and once merged with MT₁ (mid-term), from -26 to $+26$ in the case of SPIw-26 and from -26 to $+39$ for SPIw-52. The mid-term cluster MT₁,

originally indicating a period of correlation of ETDIw preceding SPIw- i from 4 to 13 weeks of aggregation, displays moderate to low but significant values of correlation (from 0.2 to 0.4) from lag -36 to -13 . The merging of the cluster ST₁ and MT₁ decreases the asymmetry defining the leading role of ETDIw over SPIw- i . The initially asymmetric interaction of ETDIw–SPIw- i that is mostly located in the negative range of lags (ST₁ and MT₁ shown between lag -30 and $+10$ for the SPIw-4 and SPIw-13 cases) propagates and dampens towards the positive range of lags with increasing aggregation. The dampening eventually shifts the interaction of ETDIw to SPIw- i from preceding to delayed (at 26 and 52 weeks of aggregation, the clusters of significant positive correlations are mostly within the positive range of lags, especially in Fig. 3d). The loss of asymmetry due to the increasing aggregation translates into an increase in the duration of the cluster as well as of the fraction of the basin significantly affected by correlations. Both effects may indicate the inconvenience of adopting long aggregation periods that alter the interaction magnitude and timing. There is an additional cluster of positive correlations, LT₁ (long-term), past 1.5 years (lags $+78$ to $+104$), particularly noticeable at SPIw-13 and SPIw-26. Blue bars in Fig. 3 indicate negative correlations for the relationship ETDIw–SPIw- i dominating the long-term between evapotranspiration and rainfall anomalies. There is a couple of clusters around lag $+42$ (tagged LT₂) and around lag $+104$ (LT₄), slightly significant, that similarly to the positive correlations, increased in duration and magnitude with the increase in the aggregation period of the SPI, particularly for SPIw-26 and SPIw-52 (Fig. 3c–d).

LSM

Results from the LSM SURFEX-ISBA (Fig. 4) show a less lasting and more concentrated cluster of significant positive correlations around lag 0 (ST₁ tagged in Fig. 4) than those observed in the RS results (Fig. 3). This result implies there is more synchronicity between the SPI and ETDI in the LSM data than in the RS data. Furthermore, the LSM provides higher magnitudes of the significant positive correlations of ETDIw–SPIw- i of ST₁ than RS results. Similarly to RS data, the duration of the highly correlated period ST₁ extends with the increasing aggregation of SPIw- i (Fig. 4a to d), eventually causing the merging of clusters ST₁ and MT₁. The initial asymmetry of the positive correlations towards the negative range of lags is due to the cluster MT₁ placed around lag -26 and cluster LT₁ (Fig. 4a and b). In the SPIw-26 and SPIw-52 cases (Fig. 4c and d) LT₁ disappears and ST₁ merges with MT₁, artificially shifting the initial asymmetry dominating the negative range of lags towards the positive range. Thus, the precedence of ETDIw with SPIw- i prevalent in the period of aggregation of 4 and 13 weeks may look like the precedence of SPIw- i with ETDIw when long aggregation periods such as the ones in SPIw-26 and SPIw-52 are applied. The

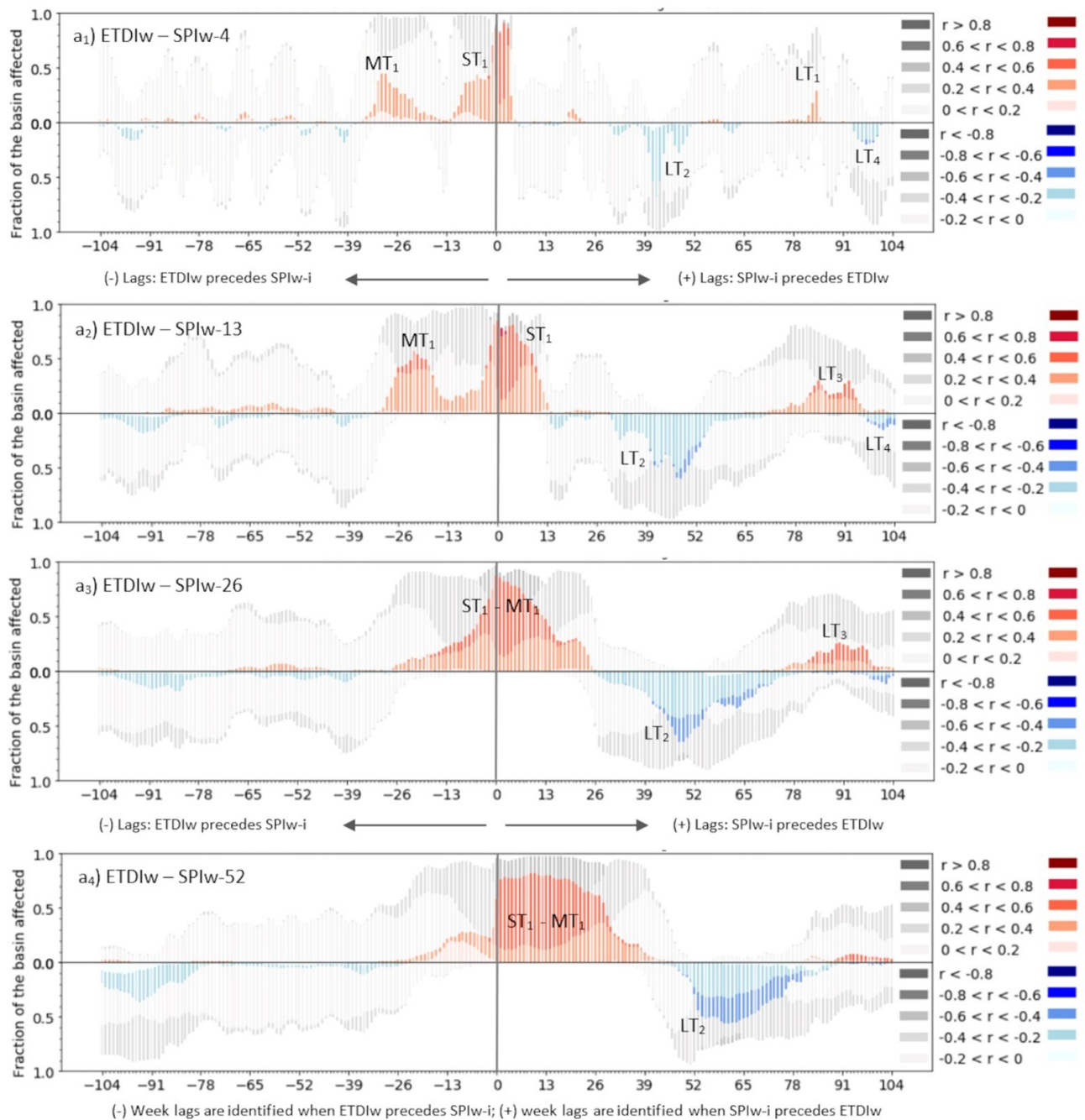


Figure 3. Lag plots of SPI-1, SPI-3, SPI-6 and SPI-12 (expressed as SPIw-4, SPIw-13, SPIw-26 and SPIw-52, respectively) with remote sensing (RS) ETDIw at the weekly scale for the period 2010–2017. Lags are calculated for the -104 leading and $+104$ lagged time steps of ETDIw in reference to SPIw- i . The height of the bars of the plot indicates the area of the basin affected by non-significant (grey scale) or significant (colored scale) correlations. The saturation of the colored scale indicates the magnitude of the significant positive (red) or negative (blue) Pearson correlation coefficient of SPIw- i and ETDIw.

initial asymmetry of the cluster ST_1 – MT_1 is lower in LSM results (Fig. 4) than in RS results (Fig. 3) due to the lower magnitude of MT_1 . The additional cluster of positive correlations, LT_3 , past the 1.5-year range of positive lags (lags $+78$ to $+104$) in LSM results (Fig. 4a to c) concurs with

that of RS results (Fig. 3a to c). LSM results (Fig. 4) show a few more clusters of negative correlations for ETDIw–SPIw- i , but these are of lower magnitude than those of RS ones (Fig. 3). These significant clusters merge with the increasing aggregation period LT_4 – LT_5 , which agrees with LT_2 shown

in RS at the 26- and 52-week period of aggregation of SPIw-*i*. LSM results further include a cluster of significant negative correlation values in the lead time range (cluster LT₂) that is absent in RS results (Fig. 4 vs. Fig. 3). The agreement between LSM and RS results confirms the asymmetrical interaction between ETDIw and SPIw-*i*. The asymmetry suggests a prevalence of the precedence of positive correlations of ETDIw with SPIw-*i* in the short term (from the monthly to the seasonal scale) while pointing to some delayed response of ETDIw to SPIw-*i* in the negative correlations in the middle to long term (from a seasonal to interannual scale). The LSM results tend to amplify the magnitude and the area affected by positive correlations compared to the RS dataset.

5.2.2 Lag analysis SPI–SMDI

RS

The interaction of SPIw-*i* with SMDIw for the RS dataset is not as strong as it was with ETDIw (Figs. 5 and 6 vs. Figs. 3 and 4). Both the correlation values and the significant fraction of the basin affected by them are lower than in the case of ETDIw. Similarly to ETDIw, the significant positive correlations around lag 0 (ST₁) are asymmetrical. Because of this, SMDIw tends to experience the effect of the preceding conditions of SPIw-*i* less than influencing those of SPIw-*i*. The increasing period of aggregation of SPIw-13, SPIw-26 and SPIw-52 widens and lags the short-term influence of SPIw-*i* on SMDIw (ST₁) into a short-term to mid-term influence (ST₁–MT₁). This widened cluster of positive correlations stays almost entirely in the positive range of lags, which differs from that of ETDIw where the ST₁–MT₁ cluster extends in both positive and negative ranges of the lags (Fig. 5 compared to Figs. 3 to 4). The leading range of lags (from lag –104 to lag 0) does not show relevant clusters of significant correlation at all, neither in the middle nor in the long term. Negative correlations of the SMDIw–SPIw-*i* interaction only occasionally stand up at a small cluster (LT₁, Fig. 5b–d) in the positive range of lags (when SPIw-*i* precedes SMDIw). The smoothing effect of the aggregation period of SPIw-*i* increasingly alters the initial bias of interactions towards the leading influence of the SMDI on SPIw, as well as delays most clusters similarly to the case with ETDIw.

LSM

The LSM results for the SMDIw–SPIw-*i* relationship depict strongly dampened patterns of significant correlation between SMDIw and SPIw-*i* compared to those of RS SMDIw–SPIw-*i* or ETDIw–SPIw-*i*. Only the ST₁ cluster is noticeable around lag 0. The increase in the aggregation period does not favor its permanence as a relevant cluster beyond SPIw-4. The cause can be the generalized low values of both non-significant and significant correlations obtained for these estimates of the LSM SURFEX-ISBA, which may

indicate the difficulties the LSM has to describe the response of the surface soil moisture (the SMDI) to the atmospheric forcing (the SPI) that we saw in the RS dataset. The periods identified of short-term, mid-term and long-term influence of one SPIw-*i* in SMDIw such as ST₁, MT₁ or LT₁ cannot be recognized in Fig. 6 compared to Fig. 5. Therefore, the LSM results of the SPIw-*i*–SMDIw relationship strongly differ from the ones obtained from RS data and are a matter of debate in the Discussion section.

5.2.3 Lag analysis ETDI–SMDI

RS

The remaining interaction in this analysis is the ETDI–SMDI. The results show a less asymmetric relationship between the ETDI and the SMDI compared to the ones of SPIw with the ETDI and SMDI. The significant moderate positive correlation values (red bars in Fig. 7a) between lag 0 and +13 and from lag –10 to 0 indicate that the influence of the ETDI on the SMDI lasts longer than the one of the SMDI on the ETDI. The magnitude, though, expresses that the SMDI moderately impacts the short-term conditions of the ETDI for about a month in comparison to the sole week the ETDI affects moderately those of the SMDI. However, the highest correlations occur for the lag –1 when the SMDI precedes the ETDI by 1 week. Negative clusters (MT₁, MT₂) at +39 and –39 weeks suggest that the interaction between the indices goes beyond the seasonal scale commented on above. However, the significance of all these mid-term to long-term clusters remains low.

LSM

The results of ETDI–SMDI interaction based on LSM data show less evident periods of interaction between the indices compared to the RS results. The expected strong correlation around lag 0 is largely diminished. The strongest cluster appears from lag –21 to –39, MT₁ (Fig. 7b), when the SMDI precedes the ETDI. No notable negative clusters can be identified. Apart from the lack of agreement on the symmetry of the interaction between LSM and RS results (Fig. 7b vs. a), the notable cluster ST₁ in RS results is less relevant in LSM results. Given the disparity between LSM and RS results, we raise concerns about the accuracy of offline LSM simulations compared to the RS results, addressing them in the next section.

6 Discussion

Results require careful discussion regarding three main aspects: firstly, the effect of adopting the weekly scale for drought indices and analyses, secondly the meaning behind the complex interactions between drought indices, and thirdly the comparison of RS and LSMs as tools for high-

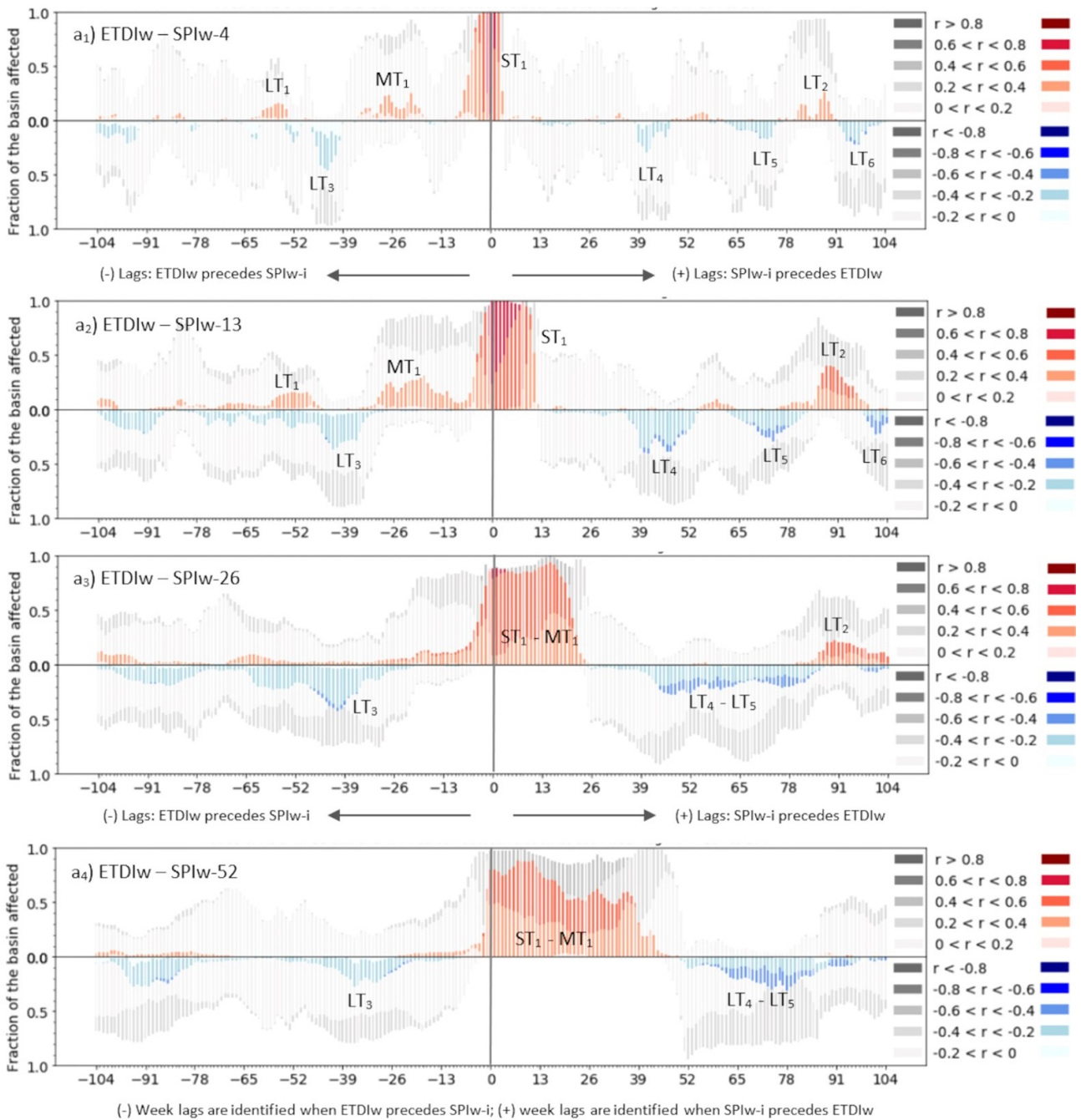


Figure 4. Lag plots of SPI-1, SPI-3, SPI-6 and SPI-12 (expressed as SPIw-4, SPIw-13, SPIw-26 and SPIw-52, respectively) with the land-surface model (LSM) ETDIw index at the weekly scale for the period 2010–2017. Lags are calculated for the –104 leading and +104 lagged time steps of ETDIw in reference to SPIw-*i*. The height of the bars of the plot indicates the area of the basin affected by non-significant (greyscale) or significant (colored scale) correlations. The saturation of the colored scale indicates the magnitude of the significant positive (red) or negative (blue) Pearson correlation coefficient of SPIw-*i* and ETDIw.

resolution monitoring of drought. All comments refer to the results on a weekly scale.

6.1 Scales for drought monitoring in semi-arid environments

Analyzing the differences in correlations between indices at monthly and weekly scales (Fig. 2), we support the neces-

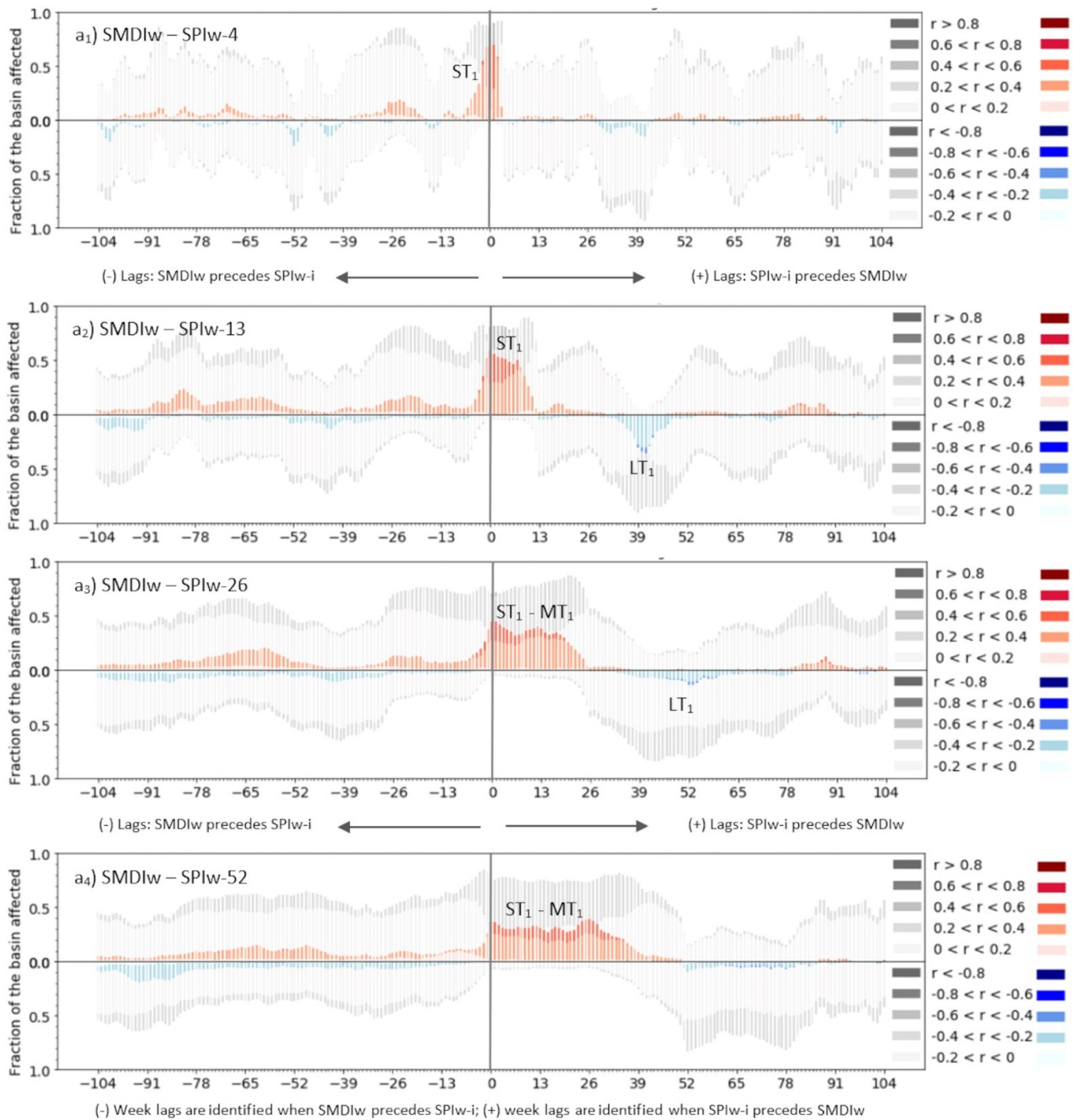


Figure 5. Lag plots of SPI-1, SPI-3, SPI-6 and SPI-12 (expressed as SPIw-4, SPIw-13, SPIw-26 and SPIw-52, respectively) with the remote sensing (RS) SMDIw index at the weekly scale for the period 2010–2017. Lags are calculated for the -104 leading and $+104$ lagged time steps of SMDIw in reference to SPIw- i . The height of the bars of the plot indicates the area of the basin affected by non-significant (greyscale) or significant (colored scale) correlations. The saturation of the colored scale indicates the magnitude of the significant positive (red) or negative (blue) Pearson correlation coefficient of SPIw- i and SMDIw.

sity of adopting the weekly scale to study lags. The monthly scale preferred for drought assessment from a hydrological perspective may overlook the quick response of the land–atmosphere interactions. The clusters of moderate to high correlation between indices mostly occur within the first

month preceding or following an anomaly (Figs. 3–7), particularly in the short to very short term. High correlations tend to peak and plunge in an interval of a few weeks. This short-term response recommends the use of the weekly scale and aggregation periods below the seasonal scale, such as SPIw-

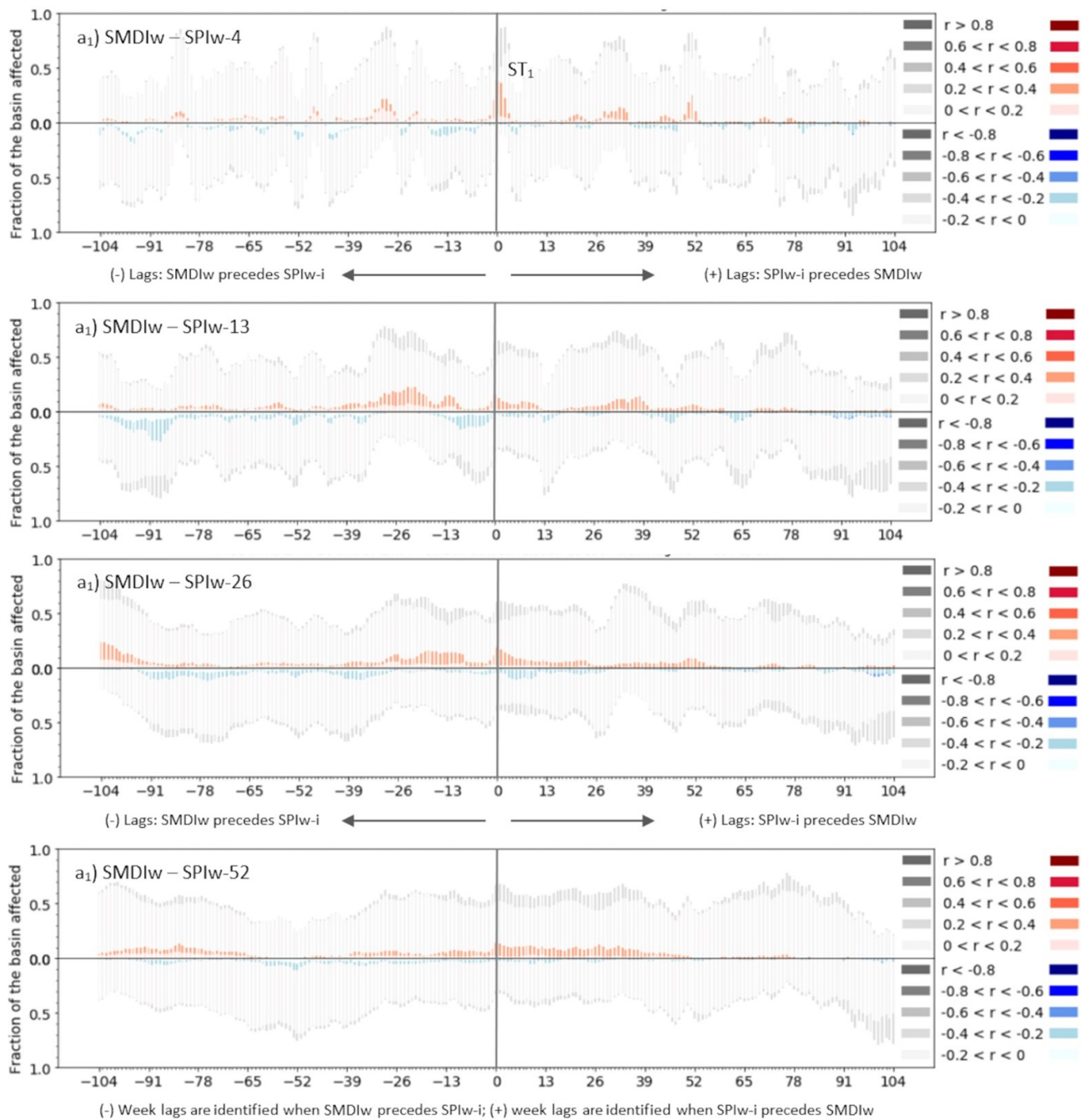


Figure 6. Lag plots of SPI-1, SPI-3, SPI-6 and SPI-12 (expressed as SPIw-4, SPIw-13, SPIw-26 and SPIw-52, respectively) with the land-surface model (LSM) SMDIw index at the weekly scale for the period 2010–2017. Lags are calculated for the –104 leading and +104 lagged time steps of SMDIw in reference to SPIw-*i*. The height of the bars of the plot indicates the area of the basin affected by non-significant (greyscale) or significant (colored scale) correlations. The saturation of the colored scale indicates the magnitude of the significant positive (red) or negative (blue) Pearson correlation coefficient of SPIw-*i* and SMDIw.

13 (equivalent to SPI3), to evaluate the delay or precedence between indices.

Our results showing soil moisture response to rainfall (–5 to 5 weeks) and evapotranspiration (–10 to 5 weeks) anomalies in a matter of weeks are consistent with pre-

vious works showing soil moisture echoes rainfall anomalies in a range from days to weeks (Scaini et al., 2015; Martínez-Fernández et al., 2016) and also when driven by evapotranspiration (Otkin et al., 2013). Therefore, in a basin exposed to the high-energy characteristics of semi-arid cli-

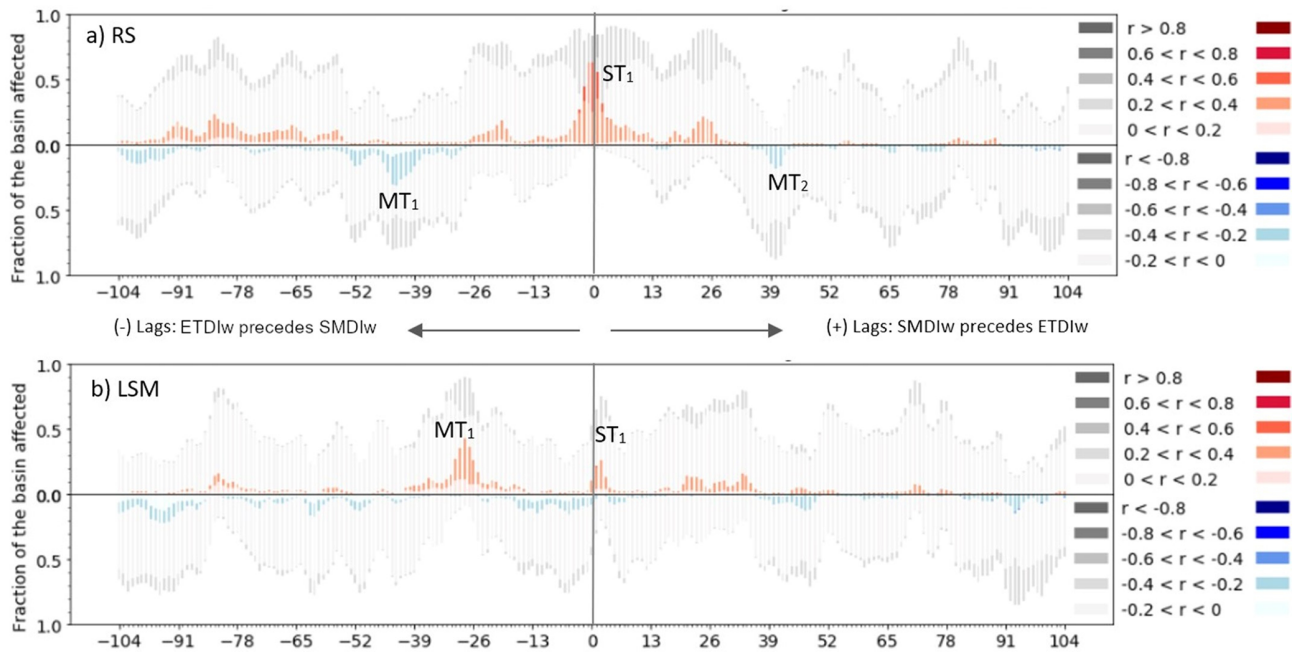


Figure 7. Lag plots of ETDI–SMDIw at the weekly timescale in the period 2010–2017 for (a) RS data and (b) LSM data. Lags are calculated for the -104 leading and for the $+104$ lagged time steps of SMDIw in reference to ETDIw. The five levels of red and blue indicate the positive (red) or negative (blue) Pearson correlation coefficient between ETDIw and SMDIw for each time step (lead or lag time step). The height of the bars of the plot indicates the area of the basin affected by that level of r Pearson values.

mates, the weekly scale allows us to diagnose disregarded short-term interactions, such as the ones of the ETDI and SMDI on the SPI, without losing resolution in the identification of mid-term to long-term interactions. The need to apply a weekly scale to the SPI, which is barely used below the monthly scale, is recommended not only for the analysis of rainfall–evapotranspiration interactions but also for soil moisture ones, which are often assessed over the monthly scale. Using the weekly scale for drought assessment demands an increase in spatial resolution. This is the reason why LSMs using coarse inputs, such as the semi-aggregated physical characteristics of the basin, may generate results with scale effects. In fact, scale effects due to the coarse resolution of the spatial characteristics can increase the temporal scale at which the processes are effectively correlated (Rodríguez-Iturbe et al., 2001). Therefore, lag analysis needs to compile datasets of appropriate spatial and temporal scales for their aims, like the high-resolution RS datasets evaluated in this study or LSM ones based on completely distributed data.

6.2 Interpretation of the interactions between drought indices

Adopting specific drought indices for rainfall, evapotranspiration and soil moisture allows exploring the interactions between variables of different levels of the land–atmosphere system. The pertinence of using the SPI, ETDI and SMDI

to evaluate the interactions between the variables’ anomalies can be the subject of discussion depending on the specific advantages, drawbacks and applicability of each index. There can be alternative drought indices even for soil moisture and evapotranspiration of better stability and statistical characteristics worth exploring. Furthermore, assessing the interactions of anomalies may be possible without using drought indices. However, since the commonplace in the analysis of the anomalies behind drought has been widely based on drought indices for comparable interpretation, we consider the SPI, ETDI and SMDI to represent a set of comprehensive indices to flexibly evaluate interactions at different timescales.

Figure 8a and graphically Fig. 8b summarize the annual mode of interactions between the SPI, ETDI and SMDI. In the short to middle term, both the ETDI and the SMDI interactions with the SPI concur on having moderate significance, with only a few negative and positive low interactions in the middle to long term. Positive correlations around lag 0 of the ETDI and SMDI with the SPI indicate direct precedent dependence of the indices, which means changes on the ETDI and SMDI correlate positively (negatively) to positive (negative) changes on the SPI. The short-term correlations after rainfall for both the ETDI and the SMDI (lagged response of these indices to the SPI) are straightforward and have been reported before in similar Iberian regions (Martínez-Fernández et al., 2016). Sustained dry or wet anomalies in both variables favored by a positive correlation between indices are primarily restricted to a length of three seasons.

Correlations beyond the year may represent the multi-annual persistence of anomalies common in Mediterranean climates.

The strong aggregation impact occurring when adopting SPIw-26 and SPIw-52 indicates the analysis of interactions may be uncertain when indices are aggregated beyond the seasonal scale. It is evaluated if the magnifying effect of clusters with long aggregation periods (SPIw-26 and SPIw-52) is the autocorrelation of the indices. Significant autocorrelated values always extend for less than the period of aggregation of SPIw-*i* (2 weeks on SPIw-1, 3 weeks on SPIw-4, 10 weeks on SPIw-13, 18 weeks on SPIw-26, 35 weeks on SPIw-52, 40 weeks on SPI-78, 45 weeks on SPIw-104). Hence, we presume autocorrelation values of the SPI series are only partly caused by the period of aggregation. The partial autocorrelation of both the ETDI and the SMDI shows mostly two significant lags, which indicate the existence of an autoregressive model of type AR(2) (Fig. S2). An AR(2) model may articulate the combination of growing and decaying factors behind the shifting balance of positive and negative correlations between indices. In this way, the clusters of interactions identified in Figs. 3 to 7 can be attributed to interactions between rainfall, evapotranspiration and soil moisture anomalies. Conversely, clusters identified in series with a period of aggregation over the seasonal scale may be misleading for the analysis of drought interactions in Mediterranean environments. Thus, drought evolution in semi-arid environments can be considered an expression of quick exchanges between land–atmosphere variables which develop within the seasonal scale. This implies the temporal resolution of drought indices must adopt short timescales (i.e., weekly scale) to capture the onset of drought.

The existence of the precedent influence of the ETDI and SMDI on the SPI (clusters of the negative range of lags) implies some unequal reciprocity (feedback) between evapotranspiration and soil moisture with rainfall. This precedent influence is weaker than the influence of the SPI on subsequent ETDI and SMDI anomalies (lagged response) but still remarkable. It is reasonable that the lagged response of evapotranspiration and soil moisture to rainfall is stronger and longer-lasting than the precedent influence (Fig. 8a). Furthermore, the precedent influence period between the ETDI and SPI is stronger and of longer duration than the one of the SMDI on the SPI. This asymmetry suggests that the ETDI, more than the SMDI, has a weekly to seasonal precedent influence on rainfall (Fig. 8b). We expected a longer period of positive correlations of the SMDI influencing rainfall, given the multiple reports of soil moisture inducing memory at the near-surface atmosphere (Manning et al., 2018).

One reason why the ETDI shows a longer influence on the SPI than the SMDI may be that the ETDI from MOD16A2 is fed by the whole depth of soil moisture, while the SMDI based on SMOS1km is limited to the top 5 cm of soil moisture, a very exposed soil level in semi-arid climates. The complexity of soil moisture dynamics, which barely follow a cyclic interaction (Rodríguez-Iturbe et al., 1991), can also

explain a weaker relationship between the SMDI and SPI compared to the ETDI. Other reasons for this may lie in the prevalence of maritime advection as the main contributor to evapotranspiration in the IP (Gimeno et al., 2010) compared to the prevalence of local soil moisture recycling common in more continental areas of Europe (Bisselink and Dolman, 2008). The advective explanation is supported by the contrast between the few weeks of precedent influence of soil moisture on rainfall we observe in the Ebro basin and the up to 250 d of precedent influence of continental areas prone to soil moisture recycling (Rowntree and Bolton, 1983; Bisselink and Dolman, 2008). Some studies focused on continental climates of relevant summer rainfall have described the implications of the alteration of the recycling due to soil moisture depletion during heat waves and drought which can eventually alter the atmosphere (Rasmijn et al., 2018; Miralles et al., 2019). In the Mediterranean climate of the Iberian Peninsula characterized by a lack of summer rainfall, soil moisture annually reaches such low levels that we can expect annual summer alterations in the near atmosphere. Differences between areas where soil moisture plays a role, like central Europe, and areas where soil moisture is unable to control the evolution of the system under high-energy conditions, like the Iberian Peninsula, have been reported before in Mediterranean-like Western Australia (Herold et al., 2016).

In consequence, our results at the Ebro basin seem compatible with the frequent activation of a reinforcing or self-intensification loop (Brubaker and Entekhabi, 1996), by which the precedent influence of negative (eventually positive) anomalies of evapotranspiration reducing (increasing) rainfall cascades into a depletion (rise) in soil moisture that further limits (enhances) the response of evapotranspiration and restarts the cycle (Fig. 8c, right column). The weak precedence of soil moisture on rainfall compared to that of evapotranspiration expresses the limited duration of the control capacity of the soil moisture over evapotranspiration in semi-arid climates of the Mediterranean type (left column of Fig. 8c). Negative correlations when indices differ in sign ($r < 0$ conditions, Fig. 8a) can be indicative of transitional periods of mid-seasons. The sharp shift from the cluster of short-term positive correlations to the cluster of mid-term to long-term negative correlations suggests a limit in the persistence of the self-intensification mechanism. A physical interpretation of the shift may be related to the change in the dominance of the sequence from the one under high-energy conditions (Fig. 8c, right column) to the one under low-energy conditions (Fig. 8c, left column). A low-energy inhibiting mechanism of negative correlations between soil moisture and surface temperature under low temperatures has already been described by Brubaker and Entekhabi (1996). Given the direct link between evapotranspiration and temperature, the shift from positive to negative interactions happening at timescales over the semester but below the yearly scale suggests that the arrival of winter low-energy condi-

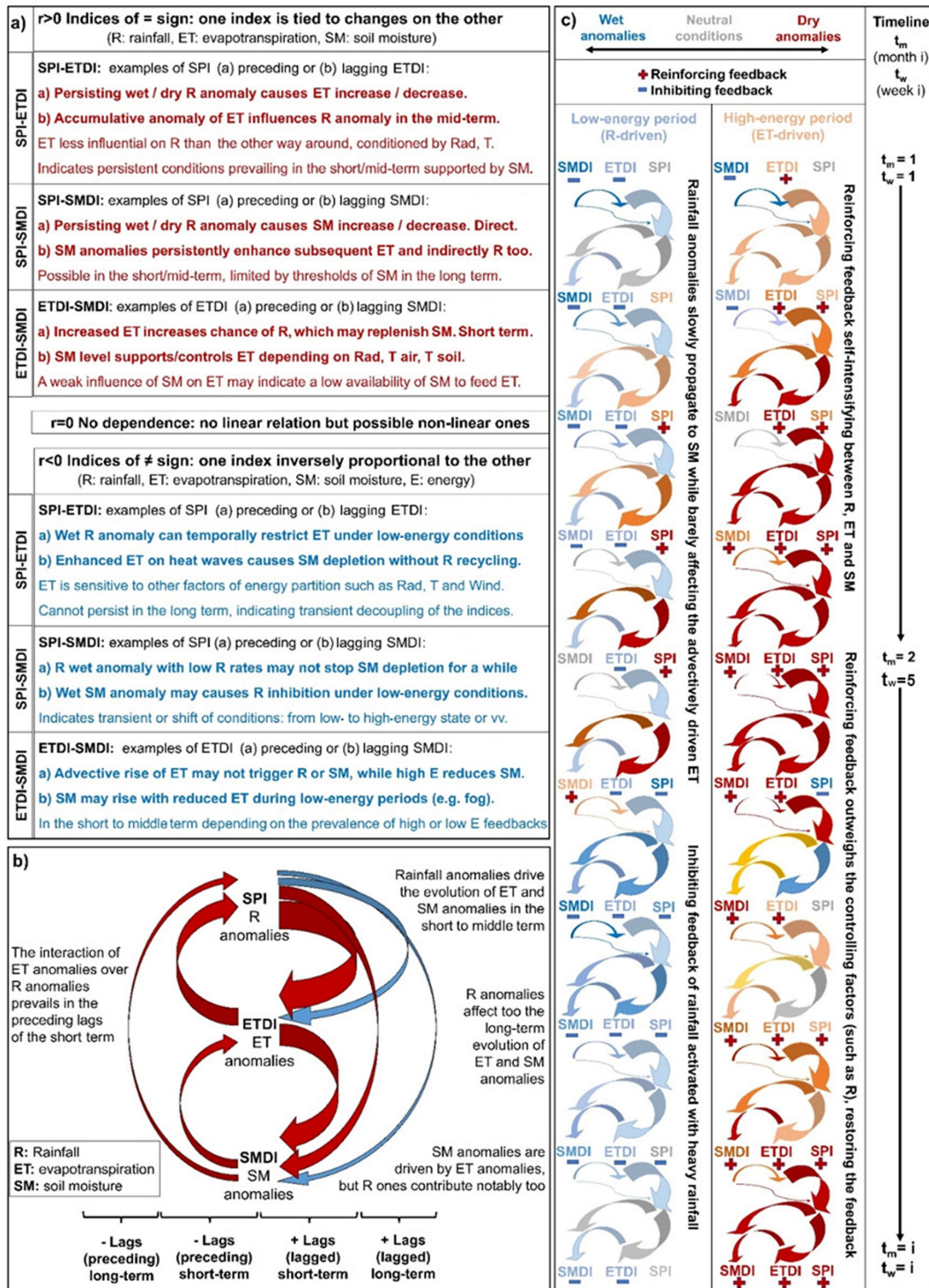


Figure 8. (a) Interpretation of the correlations between the SMDI–SPI, ETDI–SPI and SMDI–ETDI. The $r > 0$ box exemplifies positive correlations between the indices (positive correlations of red arrows in panel b), while the $r < 0$ box defines the negative ones (negative correlations of blue arrows in panel b). The abbreviation “vv” denotes vice versa. (b) Summary of the annual magnitude and timing of the interactions. Red arrows represent positive correlations and blue arrows the negative ones. Arrow width represents the magnitude of the correlation. Arrow direction determines the direction of the interaction. The timeline at the bottom indicates the scale of the interactions ranging from short-term to long-term. (c) Sequences of prevalent reinforcing (upper) and inhibiting (lower) conditions alternating during the annual cycle based on the scheme of interactions described in panels (a) and (b). The upper sequence is the self-intensifying loop driven by evapotranspiration under high-energy conditions. The lower sequence displays the inhibiting role of rainfall and soil moisture under low-energy conditions.

tions terminates the dominance of the self-intensifying loop of evapotranspiration.

In this way, the annual cycle can be modeled as the seasonal succession of two sequences: one under the low-energy conditions of winter when evapotranspiration no longer outweighs the inhibiting of soil moisture due to rainfall (left column of Fig. 8c) and the other under high-energy conditions driven by evapotranspiration (right column of Fig. 8c). The shift between the long period of interactions dominated by evapotranspiration (right column of Fig. 8c) and a short period of interactions controlled by rainfall and soil moisture (lower sequence of Fig. 8c) is generally driven by an energy threshold. However, certain levels of rainfall and soil moisture anomalies may temporally advance or delay the shift. This reason explains why under high-energy conditions drought may terminate due to heavy rainfall, while soil moisture deficits under low-energy conditions may cause an anticipated onset of the self-intensification loop of evapotranspiration.

The conceptualization of the interactions illustrated in Fig. 8 aims to raise awareness about the power of evapotranspiration anomalies to alter the land–atmosphere system, year-round, beyond hydrometeorological extremes (Seneviratne et al., 2006; Otkin et al., 2013; Teuling, 2018; Miralles et al., 2019). Another reason for supporting the year-round implications of the dominance of evapotranspiration over soil moisture is that rainfall mostly transfers to evapotranspiration in semi-arid climates (Rodríguez-Iturbe et al., 2001), where the often underestimated interception (Savenije et al., 2004) further increases evaporation at the expense of soil moisture. Additionally, as the semi-arid Mediterranean climate likely presents thresholds of rainfall, evapotranspiration and soil moisture anomalies different from those triggering hydrometeorological extremes in other areas (Tramblay et al., 2021), the evapotranspiration-dominated sequence may initiate not only more often but also more abruptly than in regions of lower-energy inputs. All these aspects, together with the increasing chance of extremes in the Mediterranean area due to climate change (Samaniego et al., 2018), recommend assessing changes in the balance of land–atmosphere interactions from the basis of this study.

However, we bear in mind that our results may oversimplify the causality, since processes not analyzed in this study may also play a role. The multiple periods showing neither prevalently positive nor prevalently negative correlations between indices indicate a loss of linear interaction. A source of non-linearity is vegetation due to its mediating role in water exchanges of the land–atmosphere system. Plants can control evapotranspiration and soil moisture in adaptation to water stress in non-linear manners that depend more on the type of vegetation (Katul et al., 2012), particularly within the Mediterranean floras (Boulet et al., 2020), than on the evapotranspiration or soil moisture status. Vegetation can also modulate the partitioning of energy governing evapotranspiration (Lansu et al., 2020) but similar processes are reported

with soil moisture (Barbeta et al., 2015). In consequence, the quick response to drought of rainfed crops and sclerophyllous vegetation (Vicente-Serrano et al., 2019) may obscure the interpretation of the links between rainfall, evapotranspiration and soil moisture. This is of concern regarding the ETDI and SMDI results because interactions of vegetation integrate the status of the atmospheric and the land-surface variables (Peters et al., 1991). Nonetheless, additional factors of uncertainty may arise from teleconnections such as the well-known North Atlantic Oscillation (NAO) or Western Mediterranean Oscillation (WeMO; Barnston and Livezey, 1987; Conte et al., 1989) or the oceanic ones like the Atlantic Multidecadal Oscillation (AMO; Kerr, 2000) altering the land–atmosphere system at large scales.

6.3 The value of remote sensing and land-surface model estimates

The RS and LSM results of the lag analysis of the ETDI–SPI interactions show consistently comparable results in contrast to the remarkable disagreement between RS and LSM results for the SMDI–SPI interaction. Results of the SMDI obtained with the LSM show substantially lower correlations than the ones of RS while also differing in the timing of the clusters of correlation. We expected the opposite, i.e., that the LSM, being simpler than reality, has stronger SPI–ETDI–SMDI correlations than the RS dataset. We assume the implicit accumulation of uncertainties in modeling (Rodríguez-Iturbe et al., 1991), partly inherited from inputs but also from the LSM structure, is the cause of the decrease in correlations. This is particularly true for soil moisture, a variable integrating exchanges between climate, soil and vegetation (Rodríguez-Iturbe et al., 2001). Secondly, this is an offline simulation, where the atmosphere (SAFRAN) is forcing the land surface (SURFEX-ISBA) without explicit feedback of SURFEX-ISBA influencing SAFRAN back. SAFRAN estimates real conditions by ingesting observations, so the feedback is implicit in results, which may be insufficient to represent reality. Thirdly, the model itself does not consider important processes like the interactive response of vegetation. ISBA has an interactive vegetation module (ISBA-A-gs), but Mediterranean vegetation can be particularly challenging for it. We expect to test the capabilities of interactive modeling vegetation in a follow-up study. Uncertainties in ISBA with vegetation also have roots in the use of the ECOCLIMAP-II database, which shows inaccuracies in cover type and the LAI. ECOCLIMAP assumes the maximum/minimum LAI occurs in June/February in contrast with the early spring and autumn LAI maximums characteristic of the Mediterranean environment (Queguiner et al., 2011). All in all, the differences between the LSM and RS datasets are already an important result to improve the LSM and comprise a useful insight into the use of offline LSM drought simulations.

Our results positively verify that RS represents an effective tool to overcome the problem of sparsely observed

soil moisture or evapotranspiration, whose crucial role in drought evolution requires high-resolution data similarly to precipitation (AghaKouchak and Nakhjiri, 2012). Including high-resolution evapotranspiration products from MODIS (MOD16A2) and soil moisture from SMOS missions (SMOS1km) together with the distributed rainfall re-analysis data allows dedicated interpretation of the interactions between these two drought-relevant variables and rainfall and their role in the water balance of the land–atmosphere interface (Dai, 2011). Especially for evapotranspiration, the maps and series of the LSM SURFEX-ISBA are comparable to those of RS, which supports the reliability of LSMs despite their limited capability in arid regions (De Kauwe et al., 2015).

The temporal and spatial patterns of the anomalies are overly identified by both RS and the LSM. The RS data seem able to capture a more complex scheme of interactions than the LSM, despite the intrinsic data issues of the RS sensors and the performance of the algorithms used to generate the products. Conversely, the LSM seems sensitive to uncertainties from input data, especially surface properties, and the offline forcing. The parametrization of the model assumes a semi-distributed approach by sub-basins of the catchment on which each sub-basin is defined based on average values of land cover and soil characteristics of the ECOCLIMAP database, which may induce some patchiness of LSM results compared to the RS results. The offline run means that the meteorological data force the LSM, but the feedbacks are lost beyond the meteorological observations included as observation in the model. Additional aspects can be, for instance, the impact of groundwater redistributing soil moisture depending on topography, which is underrepresented in the LSM. Limitations of LSMs have been reported in multiple works before and are the subject of improvement efforts (Teuling et al., 2006; Samaniego et al., 2018). Either way, uncertainties are causes of major concern in the lag analysis where they can alter the correlations between indices and obscure the interpretation of the interactions.

These aspects together can be critical to improving evapotranspiration and soil moisture estimates (Ukkola et al., 2016). Solving these inaccuracies would increase the value of RS and LSM estimates. This study exemplifies the potential of high-resolution RS and LSM products for a wide range of applications, such as drought analysis.

7 Conclusions and perspectives

The analysis of droughts in the Ebro basin using dedicated evapotranspiration and soil moisture drought indices based on high-resolution data from MOD16A2, SMOS1km and the LSM SURFEX-ISBA provides the following insights.

The monthly scale commonly adopted for drought evaluation (e.g., SPI-3) may overlook the quick evolution of drought from an agricultural and environmental perspective,

especially in the high-energy climates of the Mediterranean basin where the anomalies of rainfall, evapotranspiration and soil moisture can vary in a matter of days. The ETDI shows the strongest response at a weekly scale while it also remains influential in the mid-term. The SMDI can also quickly evolve with anomalies of evapotranspiration and particularly with lasting anomalies of rainfall. The weekly scale is advantageous to describe trends and shifts in the evolution of the indices and to identify disregarded interactions such as the preceding influence of the ETDI on the SPI.

The ETDI and SMDI, together with the SPI adapted to the weekly scale, allow tracking of the evolution of the anomalies of evapotranspiration, soil moisture and rainfall, as well as their interactions driving water anomalies in the region. There is great consistency between the time series of the ETDI, SMDI and SPI. Lag analysis between these indices clarifies the interactions between anomalies on different levels of the surface–atmosphere system, information that is neglected when using multivariable indices or indices aggregated beyond the seasonal scale. The lag analysis also identifies sequences of interactions defining reinforcing or inhibiting feedbacks. Evapotranspiration dominates the water balance of the Iberian semi-arid climate, especially during high-energy periods. This dominance frequently exceeds the controlling action of rainfall and soil moisture, inducing the reinforcing dry loop. Because of the relevance of evapotranspiration, heat waves further fueling dry events deserve further attention. The weak influence of soil moisture on subsequent evapotranspiration and rainfall limits its capability to control the propagation of anomalies.

RS datasets of MOD16A2 and SMOS-1km accurately estimate the temporal and spatial anomalies in the basin. Evapotranspiration from the LSM SURFEX-ISBA closely resembles the RS one of MOD16A2. Results differ substantially between SMOS1km and SURFEX-ISBA estimates of soil moisture. RS uncertainties arise mainly from data gaps. Land-surface model's estimates can extend the evaluation of soil moisture beyond the surface towards the root zone but face notable challenges from offline simulation neglecting feedback, as well as from the quality of input data that define surface characteristics. RS outcompetes the LSM in its ability to integrate information about challenging processes, such as vegetation dynamics. Assimilation seems the way forward to integrate the best aspects of both kinds of data. For as long as ground-based observations remain sparse, RS and LSMs represent effective tools to assess the water anomalies of the land–atmosphere system and their interaction mechanisms.

Code availability. Codes (as Python scripts) used to analyze the data are available upon request.

Data availability. Several datasets were used for this article.

- The satellite-derived evapotranspiration data of MOD16A2 are available at the Land Processes Distributed Active Archive Center (LP-DAAC) of NASA USGS at <https://lpdaac.usgs.gov/products/mod16a2v006/> (USGS 2022).
- The satellite-derived soil moisture data of SMOS1km will be available soon in repositories but are currently available upon request. The authors refer interested readers to the following publications for a detailed description of the data: Escorihuela and Quintana-Seguí (2016) and Merlin et al. (2013).
- The SAFRAN dataset forcing the SURFEX LSM simulations for Spain is being updated for ongoing studies related to this article but can be made available upon request. The last version of the SAFRAN dataset in repositories is available at the MISTRALS HyMeX database: <https://doi.org/10.14768/MISTRALS-HYMEX.1388> (Quintana-Segui, 2015). The SURFEX LSM simulations were produced for this study but can be reproduced using the corresponding release of the models: <https://www.umr-cnrm.fr/surfex/spip.php?rubrique> (CNRM, 2022).

The study followed standard statistical routines that can be easily reproduced by the methodological explanations in the text.

Supplement. The supplement related to this article is available online at: <https://doi.org/10.5194/nhess-22-3461-2022-supplement>.

Author contributions. PQS defined the research aim and together with JG collected, curated and analysed the data. MJE provided the SMOS1km dataset and supervised its integration in the study. JG and PQS analyzed the interactions between indices and the lag analysis. JG, PQS and MJE evaluated and discussed the results. JG and PQS prepared the manuscript. MJE, AB and MCLL provided feedback and improvements to the text and to the interpretation and discussion of results.

Competing interests. At least one of the (co-)authors is a member of the editorial board of *Natural Hazards and Earth System Sciences*. The peer-review process was guided by an independent editor, and the authors also have no other competing interests to declare.

Disclaimer. Publisher's note: Copernicus Publications remains neutral with regard to jurisdictional claims in published maps and institutional affiliations.

Acknowledgements. The authors acknowledge support from the Spanish State Research Agency (AEI) to the Hydrology and Climate Change lab of Pere Quintana-Seguí at Ebro Observatory.

Financial support. This research has been supported by the Spanish State Research Agency (Agencia Estatal de Investigación, AEI) within the HUMID project (AEI/FEDER EU grant no. CGL2017-85687-R).

Review statement. This paper was edited by David J. Peres and reviewed by Emanuele Romano and one anonymous referee.

References

- AghaKouchak, A. and Nakhjiri, N.: A near real-time satellite-based global drought climate data record, *Environ. Res. Lett.*, 7, 044037, <https://doi.org/10.1088/1748-9326/7/4/044037>, 2012.
- AghaKouchak, A., Farahmand, A., Melton, F. S., Teixeira, J., Anderson, M. C., Wardlow, B. D., and Hain, C. R.: Remote sensing of drought: Progress, challenges and opportunities, *Rev. Geophys.*, 53, 452–480, <https://doi.org/10.1002/2014RG000456>, 2015.
- Avissar, R. and Pielke, R. A.: A parameterization of heterogeneous land surfaces for atmospheric numerical models and its impact on regional meteorology, *Mon. Weather Rev.*, 117, 2113–2136, [https://doi.org/10.1175/1520-0493\(1989\)117<2113:APOHLS>2.0.CO;2](https://doi.org/10.1175/1520-0493(1989)117<2113:APOHLS>2.0.CO;2), 1989.
- Barbeta, A., Mejía-Chang, M., Ogaya, R., Voltas, J., Dawson, T. E., and Peñuelas, J.: The combined effects of a long-term experimental drought and an extreme drought on the use of plant-water sources in a Mediterranean forest, *Glob. Change Biol.*, 21, 1213–1225, <https://doi.org/10.1111/gcb.12785>, 2015.
- Barella-Ortiz, A. and Quintana-Seguí, P.: Evaluation of drought representation and propagation in regional climate model simulations across Spain, *Hydrol. Earth Syst. Sci.*, 23, 5111–5131, <https://doi.org/10.5194/hess-23-5111-2019>, 2019.
- Barker, L. J., Hannaford, J., Chiveron, A., and Svensson, C.: From meteorological to hydrological drought using standardised indicators, *Hydrol. Earth Syst. Sci.*, 20, 2483–2505, <https://doi.org/10.5194/hess-20-2483-2016>, 2016.
- Barnston, A. G. and Livezey, R. E.: Classification, Seasonality and Persistence of Low-Frequency Atmospheric Circulation Patterns, *Mon. Weather Rev.*, 115, 1083–1126, [https://doi.org/10.1175/1520-0493\(1987\)115<1083:CSAPOL>2.0.CO;2](https://doi.org/10.1175/1520-0493(1987)115<1083:CSAPOL>2.0.CO;2), 1987.
- Bartalis, Z., Wagner, W., Naeimi, V., Hasenauer, S., Scipal, K., Bonekamp, H., Figa, J., and Anderson, C.: Initial soil moisture retrievals from the METOP-A Advanced Scatterometer (ASCAT), *Geophys. Res. Lett.*, 34, L20401, <https://doi.org/10.1029/2007GL031088>, 2007.
- Beck, H. E., Zimmermann, N. E., McVicar, T. R., Vergopolan, N., Berg, A., and Wood, E. F.: Present and future Köppen–Geiger climate classification maps at 1-km resolution, *Scientific Data*, 5, 180214, <https://doi.org/10.1038/sdata.2018.214>, 2018.
- Bisselink, B. and Dolman, A. J.: Precipitation recycling: Moisture sources over Europe using ERA-40 data, *J. Hydrometeorol.*, 9, 1073–1083, <https://doi.org/10.1175/2008JHM962.1>, 2008.
- Boone, A., Calvet, J. C., and Noilhan, J.: Inclusion of a Third Soil Layer in a Land Surface Scheme Using the Force–Restore Method, *J. Appl. Mete-*

- orol., 38, 1611–1630, [https://doi.org/10.1175/1520-0450\(1999\)038<1611:IOATSL>2.0.CO;2](https://doi.org/10.1175/1520-0450(1999)038<1611:IOATSL>2.0.CO;2), 1999.
- Boulet, G., Jarlan, L., Olioso, A., and Nieto, H.: Chapter 2: Evapotranspiration in the Mediterranean region, in: *Water resources in the Mediterranean region*, Elsevier, 23–49, <https://doi.org/10.1016/B978-0-12-818086-0.00002-9>, 2020.
- Brubaker, K. L. and Entekhabi, D.: Analysis of feedback mechanisms in land-atmosphere interaction, *Water Resour. Res.*, 32, 1343–1357, <https://doi.org/10.1029/96WR00005>, 1996.
- CNRM: SURFEX, CNRM [data set], <https://www.umr-cnrm.fr/surfex/spip.php?rubrique>, last access: 18 October 2022.
- Conte, M., Giuffrida, S., and Tedesco, S.: The Mediterranean oscillation: impact on precipitation and hydrology in Italy, in: *Proceedings of the Conference on Climate and Water*, Vol. 1, Publications of Academy of Finland, Helsinki, 121–137, 1989.
- Dai, A.: Drought under global warming: a review, *WIREs Clim. Change*, 2, 45–65, <https://doi.org/10.1002/wcc.81>, 2011.
- Dari, J., Quintana-Seguí, P., Escorihuela, M. J., Stefan, V., Brocca, L., and Morbidelli, R.: Detecting and mapping irrigated areas in a Mediterranean environment by using remote sensing soil moisture and a land surface model, *J. Hydrol.*, 596, 126129, <https://doi.org/10.1016/j.jhydrol.2021.126129>, 2021.
- Dasari, H. P., Pozo, I., Ferri-Yáñez, F., and Araújo, M. B.: A regional climate study of heat waves over the Iberian Peninsula, *Atmospheric and Climate Sciences*, 4, 841, <https://doi.org/10.4236/acs.2014.45074>, 2014.
- David, C. H., Habets, F., Maidment, D. R., and Yang, Z. L.: RAPID applied to the SIM-France model, *Hydrol. Process.*, 25, 3412–3425, <https://doi.org/10.1002/hyp.8070>, 2011.
- Decharme, B., Boone, A., Delire, C., and Noilhan, J.: Local evaluation of the Interaction between Soil Biosphere Atmosphere soil multilayer diffusion scheme using four pedotransfer functions, *J. Geophys. Res.*, 116, D20126, <https://doi.org/10.1029/2011JD016002>, 2011.
- De Kauwe, M. G., Zhou, S.-X., Medlyn, B. E., Pitman, A. J., Wang, Y.-P., Duursma, R. A., and Prentice, I. C.: Do land surface models need to include differential plant species responses to drought? Examining model predictions across a mesic-xeric gradient in Europe, *Biogeosciences*, 12, 7503–7518, <https://doi.org/10.5194/bg-12-7503-2015>, 2015.
- Dorigo, W., Wagner, W., Albergel, C., Albrecht, F., Balsamo, G., Brocca, L., Chung, D., Ertl, M., Forkel, M., Gruber, A., Haas, E., Hamer, P. D., Hirschi, M., Ikonen, J., de Jeu, R., Kidd, R., Lahoz, W., Liu, Y. Y., Miralles, D., Mistelbauer, T., Nicolai-Shaw, N., Parinussa, R., Pratola, C., Reimer, C., van der Schalie, R., Seneviratne, S. I., Smolander, T., and Lecomte, P.: ESA CCI Soil Moisture for improved Earth system understanding: State-of-the-art and future directions, *Remote Sens. Environ.*, 203, 185–215, <https://doi.org/10.1016/j.rse.2017.07.001>, 2017.
- Durand, Y., Giraud, G., Brun, E., Merindol, L., and Martin, E.: A computer-based system simulating snowpack structures as a tool for regional avalanche forecasting, *J. Glaciol.*, 45, 469–484, <https://doi.org/10.3189/S002214300001337>, 1999.
- Entekhabi, D., Njoku, E. G., O'Neill, P. E., Kellogg, K. H., Crow, W. T., Edelstein, W. N., Entin, J. K., Goodman, S. D., Jackson, T. J., Johnson, J., Kimball, J., Piepmeier, J. R., Koster, R. D., Martin, N., McDonald, K. C., Moghaddam, M., Moran, S., Reichle, R., Shi, J. C., Spencer, M. W., Thurman, S. W., Tsang, L., and Van Zyl, J.: The soil moisture active passive (SMAP) mission, *P. IEEE*, 98, 704–716, <https://doi.org/10.1109/JPROC.2010.2043918>, 2010.
- Escorihuela, M. J. and Quintana-Seguí, P.: Comparison of remote sensing and simulated soil moisture datasets in Mediterranean landscapes, *Remote Sens. Environ.*, 180, 99–114, <https://doi.org/10.1016/j.rse.2016.02.046>, 2016.
- Escorihuela, M. J., Merlin, O., Stefan, V., Moyano, G., Eweys, O. A., Zribi, M., Kamara, S., Benahi, A. S., Ebbe, M. A. B., Chihrane, J., Ghaout, S., Cissé, S., Diakité, F., Lazar, M., Pellarin, T., Grippa, M., Cressman, K., and Piou, C.: SMOS based high resolution soil moisture estimates for desert locust preventive management, *Remote Sensing Applications: Society and Environment*, 11, 140–150, <https://doi.org/10.1016/j.rsase.2018.06.002>, 2018.
- Farahmand, A. and AghaKouchak, A.: A generalized framework for deriving nonparametric standardized drought indicators, *Adv. Water Resour.*, 76, 140–145, <https://doi.org/10.1016/j.advwatres.2014.11.012>, 2015.
- Faroux, S., Kaptué Tchuenté, A. T., Roujean, J.-L., Masson, V., Martin, E., and Le Moigne, P.: ECOCLIMAP-II/Europe: a twofold database of ecosystems and surface parameters at 1 km resolution based on satellite information for use in land surface, meteorological and climate models, *Geosci. Model Dev.*, 6, 563–582, <https://doi.org/10.5194/gmd-6-563-2013>, 2013.
- Gimeno, L., Nieto, R., Trigo, R. M., Vicente-Serrano, S. M., and López-Moreno, J. I.: Where does the Iberian Peninsula moisture come from? An answer based on a Lagrangian approach, *J. Hydrometeorol.*, 11, 421–436, <https://doi.org/10.1175/2009JHM1182.1>, 2010.
- Gudmundsson, L., Rego, F. C., Rocha, M., and Seneviratne, S. I.: Predicting above normal wildfire activity in southern Europe as a function of meteorological drought, *Environ. Res. Lett.*, 9, 084008, <https://doi.org/10.1088/1748-9326/9/8/084008>, 2014.
- Habets, F., Boone, A., Champeaux, J.L., Etchevers, P., Franchistéguy, L., Leblois, E., Ledoux, E., Le Moigne, P., Martin, E., Morel, S., Noilhan, J., Quintana-Seguí, P., Rousset-Regimbeau, F., and Viennot, P.: The SAFRAN-ISBA-MODCOU hydrometeorological model applied over France, *J. Geophys. Res.*, 113, D06113, <https://doi.org/10.1029/2007JD008548>, 2008.
- Herold, N., Kala, J., and Alexander, L. V.: The influence of soil moisture deficits on Australian heatwaves, *Environ. Res. Lett.*, 11, 064003, <https://doi.org/10.1088/1748-9326/11/6/064003>, 2016.
- Herrera-Estrada, J. E., Satoh, Y., and Sheffield, J.: Spatiotemporal dynamics of global drought, *Geophys. Res. Lett.*, 44, 2254–2263, <https://doi.org/10.1002/2016GL071768>, 2017.
- Hoerling, M., Eischeid, J., Perlwitz, J., Quan, X., Zhang, T., and Pegion, P.: On the increased frequency of Mediterranean drought, *J. Climate*, 25, 2146–2161, <https://doi.org/10.1175/JCLI-D-11-00296.1>, 2012.
- Hornacek, M., Wagner, W., Sabel, D., Truong, H. L., Snoeij, P., Hahmann, T., Diedrich, E., and Doubková, M.: Potential for high resolution systematic global surface soil moisture retrieval via change detection using Sentinel-1, *IEEE J. Sel. Top. Appl.*, 5, 1303–1311, <https://doi.org/10.1109/JSTARS.2012.2190136>, 2012.
- Jiménez, M. A., Jaksic, F. M., Armesto, J. J., Gaxiola, A., Meserve, P. L., Kelt, D. A., and Gutiérrez, J. R.: Extreme climatic events change the dynamics and invasibility of semi-

- arid annual plant communities, *Ecol. Lett.*, 14, 1227–1235, <https://doi.org/10.1111/j.1461-0248.2011.01693.x>, 2011.
- Katul, G. G., Oren, R., Manzoni, S., Higgins, C., and Parlange, M. B.: Evapotranspiration: a process driving mass transport and energy exchange in the soil-plant-atmosphere-climate system, *Rev. Geophys.*, 50, RG3002, <https://doi.org/10.1029/2011RG000366>, 2012.
- Kerr, R. A.: A North Atlantic Climate Pacemaker for the Centuries, *Science*, 288, 1984–1985, <https://doi.org/10.1126/science.288.5473.1984>, 2000.
- Kerr, Y. H., Waldteufel, P., Wigneron, J. P., Delwart, S., Cabot, F., Boutin, J., Escorihuela, M.-J., Font, J., Reul, N., Gruhier, C., Juglea, S. E., Drinkwater, M. R., Hahne, A., Martín-Neira, M., and Mecklenburg, S.: The SMOS mission: New tool for monitoring key elements of the global water cycle, *P. IEEE*, 98, 666–687, <https://doi.org/10.1109/JPROC.2010.2043032>, 2010.
- Lansu, E. M., van Heerwaarden, C. C., Stegehuis, A. I., and Teuling, A. J.: Atmospheric aridity and apparent soil moisture drought in European forest during heat waves, *Geophys. Res. Lett.*, 47, e2020GL087091, <https://doi.org/10.1029/2020GL087091>, 2020.
- Ledoux, E., Girard, G., De Marsily, G., Villeneuve, J. P., and Deschenes, J.: Spatially distributed modeling: conceptual approach, coupling surface water and groundwater, in: *Unsaturated Flow in Hydrologic Modeling*, Springer, Dordrecht, 435–454, https://doi.org/10.1007/978-94-009-2352-2_16, 1989.
- Le Moigne, P., Besson, F., Martin, E., Boé, J., Boone, A., Decharme, B., Etchevers, P., Faroux, S., Habets, F., Lafaysse, M., Leroux, D., and Rousset-Regimbeau, F.: The latest improvements with SURFEX v8.0 of the Safran–Isba–Modcou hydrometeorological model for France, *Geosci. Model Dev.*, 13, 3925–3946, <https://doi.org/10.5194/gmd-13-3925-2020>, 2020.
- Liu, W. T. and Kogan, F. N.: Monitoring regional drought using the vegetation condition index, *Int. J. Remote Sens.*, 17, 2761–2782, <https://doi.org/10.1080/01431169608949106>, 1996.
- López-Moreno, J. I., Zabalza, J., Vicente-Serrano, S. M., Revuelto, J., Gilaberte, M., Azorin-Molina, C., Morán-Tejeda, E., García-Ruiz, J. M., and Tague, C.: Impact of climate and land use change on water availability and reservoir management: Scenarios in the Upper Aragón River, Spanish Pyrenees, *Sci. Total Environ.*, 493, 1222–1231, <https://doi.org/10.1016/j.scitotenv.2013.09.031>, 2014.
- Manning, C., Widmann, M., Bevacqua, E., Van Loon, A. F., Maraun, D., and Vrac, M.: Soil moisture drought in Europe: a compound event of precipitation and potential evapotranspiration on multiple time scales, *J. Hydrometeorol.*, 19, 1255–1271, <https://doi.org/10.1175/JHM-D-18-0017.1>, 2018.
- Martens, B., Miralles, D. G., Lievens, H., van der Schalie, R., de Jeu, R. A. M., Fernández-Prieto, D., Beck, H. E., Dorigo, W. A., and Verhoest, N. E. C.: GLEAM v3: satellite-based land evaporation and root-zone soil moisture, *Geosci. Model Dev.*, 10, 1903–1925, <https://doi.org/10.5194/gmd-10-1903-2017>, 2017.
- Martínez-Fernández, J., González-Zamora, A., Sánchez, N., Guzzio, A., and Herrero-Jiménez, C. M.: Satellite soil moisture for agricultural drought monitoring: Assessment of the SMOS derived Soil Water Deficit Index, *Remote Sens. Environ.*, 177, 277–286, <https://doi.org/10.1016/j.rse.2016.02.064>, 2016.
- Masson, V., Le Moigne, P., Martin, E., Faroux, S., Alias, A., Alkama, R., Belamari, S., Barbu, A., Boone, A., Bouyssel, F., Brousseau, P., Brun, E., Calvet, J.-C., Carrer, D., Decharme, B., Delire, C., Donier, S., Essaouini, K., Gibelin, A.-L., Giordani, H., Habets, F., Jidane, M., Kerdraon, G., Kourzeneva, E., Lafaysse, M., Lafont, S., Lebeaupin Brossier, C., Lemonsu, A., Mahfouf, J.-F., Marguinaud, P., Mokhtari, M., Morin, S., Pigeon, G., Salgado, R., Seity, Y., Taillefer, F., Tanguy, G., Tulet, P., Vincendon, B., Vionnet, V., and Voltaire, A.: The SURFEXv7.2 land and ocean surface platform for coupled or offline simulation of earth surface variables and fluxes, *Geosci. Model Dev.*, 6, 929–960, <https://doi.org/10.5194/gmd-6-929-2013>, 2013.
- Mausser, W. and Schädlich, S.: Modelling the Spatial Distribution of Evapotranspiration Using Remote Sensing Data and PROMET, *J. Hydrol.*, 212–213, 250–267, [https://doi.org/10.1016/S0022-1694\(98\)00228-5](https://doi.org/10.1016/S0022-1694(98)00228-5), 1998.
- McKee, T. B., Doesken, N. J., and Kleist, J.: The relationship of drought frequency and duration to time scale, in: *Proceedings of the Eighth Conference on Applied Climatology*, Anaheim, California, 17–22 January 1993, American Meteorological Society, Boston, 179–184, 1993.
- Merlin, O., Rudiger, C., Al Bitar, A., Richaume, P., Walker, J. P., and Kerr, Y. H.: Disaggregation of SMOS soil moisture in Southeastern Australia, *IEEE T. Geosci. Remote.*, 50, 1556–1571, <https://doi.org/10.1109/TGRS.2011.2175000>, 2012.
- Merlin, O., Escorihuela, M. J., Mayoral, M. A., Hagolle, O., Al Bitar, A., and Kerr, Y.: Self-calibrated evaporation-based disaggregation of SMOS soil moisture: An evaluation study at 3 km and 100 m resolution in Catalunya, Spain, *Remote Sens. Environ.*, 130, 25–38, <https://doi.org/10.1016/j.rse.2012.11.008>, 2013.
- Miralles, D. G., Holmes, T. R. H., De Jeu, R. A. M., Gash, J. H., Meesters, A. G. C. A., and Dolman, A. J.: Global land-surface evaporation estimated from satellite-based observations, *Hydrol. Earth Syst. Sci.*, 15, 453–469, <https://doi.org/10.5194/hess-15-453-2011>, 2011.
- Miralles, D. G., Gentile, P., Seneviratne, S. I., and Teuling, A. J.: Land–atmospheric feedbacks during droughts and heatwaves: state of the science and current challenges, *Ann. NY Acad. Sci.*, 1436, 19–35, <https://doi.org/10.1111/nyas.13912>, 2019.
- MMA: Libro Blanco del Agua en España, Spanish Ministry of Environment (MMA), http://www.cedex.es/CEDEX/LANG_CASTELLANO/ORGANISMO/CENTYLAB/CEH/Documents_Descargas/LB_LibroBlancoAgua.htm (last access: 18 October 2022), 2000.
- Molero, B., Merlin, O., Malbêteau, Y., Al Bitar, A., Cabot, F., Stefan, V., Kerr, Y., Bacon, S., Cosh, M. H., Bindlish, R., and Jackson, T. J.: SMOS disaggregated soil moisture product at 1 km resolution: Processor overview and first validation results, *Remote Sens. Environ.*, 180, 361–376, <https://doi.org/10.1016/j.rse.2016.02.045>, 2016.
- Monteleone, B., Bonaccorso, B., and Martina, M.: A joint probabilistic index for objective drought identification: the case study of Haiti, *Nat. Hazards Earth Syst. Sci.*, 20, 471–487, <https://doi.org/10.5194/nhess-20-471-2020>, 2020.
- Mu, Q., Zhao, M., and Running, S. W.: MODIS global terrestrial evapotranspiration (ET) product (NASA MOD16A2/A3), Algorithm Theoretical Basis Document, Collection, Vol. 5, p. 60, <https://modis-land.gsfc.nasa.gov/pdf/MOD16ATBD.pdf> (last access: 18 October 2022), 2013.
- Muñoz-Sabater, J., Dutra, E., Agustí-Panareda, A., Albergel, C., Arduini, G., Balsamo, G., Boussetta, S., Choulga, M., Harri-

- gan, S., Hersbach, H., Martens, B., Miralles, D. G., Piles, M., Rodríguez-Fernández, N. J., Zsoter, E., Buontempo, C., and Thépaut, J.-N.: ERA5-Land: a state-of-the-art global reanalysis dataset for land applications, *Earth Syst. Sci. Data*, 13, 4349–4383, <https://doi.org/10.5194/essd-13-4349-2021>, 2021.
- Narasimhan, B. and Srinivasan, R.: Development and evaluation of Soil Moisture Deficit Index (SMDI) and Evapotranspiration Deficit Index (ETDI) for agricultural drought monitoring, *Agr. Forest. Meteorol.*, 133, 69–88, <https://doi.org/10.1016/j.agrformet.2005.07.012>, 2005.
- Nogueira, M., Albergel, C., Boussetta, S., Johannsen, F., Trigo, I. F., Ermida, S. L., Martins, J. P. A., and Dutra, E.: Role of vegetation in representing land surface temperature in the CHTESSEL (CY45R1) and SURFEX-ISBA (v8.1) land surface models: a case study over Iberia, *Geosci. Model Dev.*, 13, 3975–3993, <https://doi.org/10.5194/gmd-13-3975-2020>, 2020.
- Noilhan, J. and Mahfouf, J.-F.: The ISBA land surface parameterisation scheme, *Global Planet. Change*, 13, 145–159, [https://doi.org/10.1016/0921-8181\(95\)00043-7](https://doi.org/10.1016/0921-8181(95)00043-7), 1996.
- Otkin, J. A., Anderson, M. C., Hain, C., Mladenova, I. E., Basara, J. B., and Svoboda, M.: Examining rapid onset drought development using the thermal infrared-based evaporative stress index, *J. Hydrometeorol.*, 14, 1057–1074, <https://doi.org/10.1175/JHM-D-12-0144.1>, 2013.
- Otkin, J. A., Anderson, M. C., Hain, C., and Svoboda, M.: Using temporal changes in drought indices to generate probabilistic drought intensification forecasts, *J. Hydrometeorol.*, 16, 88–105, <https://doi.org/10.1175/JHM-D-14-0064.1>, 2015.
- Pablos, M., Martínez-Fernández, J., Sánchez, N., and González-Zamora, Á.: Temporal and spatial comparison of agricultural drought indices from moderate resolution satellite soil moisture data over Northwest Spain, *Remote Sens.*, 9, 1168, <https://doi.org/10.3390/rs9111168>, 2017.
- Palmer, W. C.: Meteorological drought, U.S. Weather Bureau, Res. Pap. No. 45, 58 pp., 1965.
- Peters, A. J., Rundquist, D. C., and Wilhite, D. A.: Satellite detection of the geographic core of the 1988 Nebraska drought, *Agr. Forest Meteorol.*, 57, 35–47, [https://doi.org/10.1016/0168-1923\(91\)90077-4](https://doi.org/10.1016/0168-1923(91)90077-4), 1991.
- Queguiner, S., Martin, E., Lafont, S., Calvet, J.-C., Faroux, S., and Quintana-Seguí, P.: Impact of the use of a CO₂ responsive land surface model in simulating the effect of climate change on the hydrology of French Mediterranean basins, *Nat. Hazards Earth Syst. Sci.*, 11, 2803–2816, <https://doi.org/10.5194/nhess-11-2803-2011>, 2011.
- Quintana Seguí, P.: SAFRAN analysis over Spain, ESPRI/IPSL [data set], <https://doi.org/10.14768/MISTRALS-HYMEX.1388>, 2015.
- Quintana-Seguí, P., Le Moigne, P., Durand, Y., Martin, E., Habets, F., Baillon, M., Canellas, C., Franchisteguy, L., and Morel, S.: Analysis of near-surface atmospheric variables: Validation of the SAFRAN analysis over France, *J. Appl. Meteorol. Clim.*, 47, 92–107, <https://doi.org/10.1175/2007JAMC1636.1>, 2008.
- Quintana-Seguí, P., Peral, M. C., Turco, M., Llasat, M. C., and Martin, E.: Meteorological Analysis Systems in North-East Spain: Validation of SAFRAN and SPAN, *J. Environ. Inform.*, 27, 116–130, <https://doi.org/10.3808/jei.201600335>, 2016.
- Quintana-Seguí, P., Turco, M., Herrera, S., and Miguez-Macho, G.: Validation of a new SAFRAN-based gridded precipitation product for Spain and comparisons to Spain02 and ERA-Interim, *Hydrol. Earth Syst. Sci.*, 21, 2187–2201, <https://doi.org/10.5194/hess-21-2187-2017>, 2017.
- Quintana-Seguí, P., Barella-Ortiz, A., Regueiro-Sanz, S., and Miguez-Macho, G.: The utility of land-surface model simulations to provide drought information in a water management context using global and local forcing datasets, *Water Resour. Manag.*, 34, 2135–2156, <https://doi.org/10.1007/s11269-018-2160-9>, 2020.
- Rasmijn, L. M., Van der Schrier, G., Bintanja, R., Barkmeijer, J., Sterl, A., and Hazeleger, W.: Future equivalent of 2010 Russian heatwave intensified by weakening soil moisture constraints, *Nat. Clim. Change*, 8, 381–385, <https://doi.org/10.1038/s41558-018-0114-0>, 2018.
- Ribeiro, A. F., Russo, A., Gouveia, C. M., and Páscoa, P.: Modelling drought-related yield losses in Iberia using remote sensing and multiscalar indices, *Theor. Appl. Climatol.*, 136, 203–220, <https://doi.org/10.1007/s00704-018-2478-5>, 2019.
- Rodríguez-Iturbe, I., Entekhabi, D., and Bras, R. L.: Non-linear dynamics of soil moisture at climate scales: I. Stochastic analysis, *Water Resour. Res.*, 27, 1899–1906, <https://doi.org/10.1029/91WR01035>, 1991.
- Rodríguez-Iturbe, I., Porporato, A., Laio, F., and Ridolfi, L.: Plants in water-controlled ecosystems: active role in hydrologic processes and response to water stress: I. Scope and general outline, *Adv. Water Resour.*, 24, 695–705, [https://doi.org/10.1016/S0309-1708\(01\)00004-5](https://doi.org/10.1016/S0309-1708(01)00004-5), 2001.
- Rowntree, P. R. and Bolton, J. A.: Simulation of the atmospheric response to soil moisture anomalies over Europe, *Q. J. Roy. Meteor. Soc.*, 109, 501–526, <https://doi.org/10.1002/qj.49710946105>, 1983.
- Running, S. W., Mu, Q., Zhao, M., and Moreno, A.: MODIS global terrestrial evapotranspiration (ET) product (MOD16A2/A3 and year-end gap-filled MOD16A2GF/A3GF) NASA Earth Observing System MODIS Land Algorithm (for collection 6), National Aeronautics and Space Administration, Washington, DC, USA [data set], <https://doi.org/10.5067/MODIS/MOD16A2.061>, 2019.
- Sahoo, A. K., Sheffield, J., Pan, M., and Wood, E. F.: Evaluation of the tropical rainfall measuring mission multi-satellite precipitation analysis (TMPA) for assessment of large-scale meteorological drought, *Remote Sens. Environ.*, 159, 181–193, <https://doi.org/10.1016/j.rse.2014.11.032>, 2015.
- Saini, H. S. and Westgate, M. E.: Reproductive development in grain crops during drought, *Adv. Agron.*, 68, 59–96, [https://doi.org/10.1016/S0065-2113\(08\)60843-3](https://doi.org/10.1016/S0065-2113(08)60843-3), 1999.
- Samaniego, L., Thober, S., Kumar, R., Wanders, N., Rakovec, O., Pan, M., and Marx, A.: Anthropogenic warming exacerbates European soil moisture droughts, *Nat. Clim. Change*, 8, 421–426, <https://doi.org/10.1038/s41558-018-0138-5>, 2018.
- Sánchez, N., González-Zamora, Á., Piles, M., and Martínez-Fernández, J.: A new Soil Moisture Agricultural Drought Index (SMADI) integrating MODIS and SMOS products: A case of study over the Iberian Peninsula, *Remote Sens.*, 8, 287, <https://doi.org/10.3390/rs8040287>, 2016.
- Savenije, H. H. G.: The importance of interception and why we should delete the term evapotranspiration from our vocabulary, *Hydrol. Process.*, 18, 1507–1511, <https://doi.org/10.1002/hyp.5563>, 2004.

- Scaini, A., Sánchez, N., Vicente-Serrano, S. M., and Martínez-Fernández, J.: SMOS-derived soil moisture anomalies and drought indices: a comparative analysis using in situ measurements, *Hydrol. Process.*, 29, 373–383, <https://doi.org/10.1002/hyp.10150>, 2015.
- Schultz, K., Franks, S., and Beven, K.: TOPUP – A TOPMODEL based SVAT model to calculate evaporative fluxes between the land surface and the atmosphere, Version 1.1, Program 25 documentation, Department of Environmental Science, Lancaster University, UK, 1998.
- Seneviratne, S. I., Lüthi, D., Litschi, M., and Schär, C.: Land-atmosphere coupling and climate change in Europe, *Nature*, 443, 205–209, <https://doi.org/10.1038/nature05095>, 2006.
- Seneviratne, S. I., Corti, T., Davin, E. L., Hirschi, M., Jaeger, E. B., Lehner, I., Orlowsky, B., and Teuling, A. J.: Investigating soil moisture–climate interactions in a changing climate: A review, *Earth-Sci. Rev.*, 99, 125–161, <https://doi.org/10.1016/j.earscirev.2010.02.004>, 2010.
- Sepulcre-Canto, G., Horion, S., Singleton, A., Carrao, H., and Vogt, J.: Development of a Combined Drought Indicator to detect agricultural drought in Europe, *Nat. Hazards Earth Syst. Sci.*, 12, 3519–3531, <https://doi.org/10.5194/nhess-12-3519-2012>, 2012.
- Sousa, P. M., Trigo, R. M., Aizpurua, P., Nieto, R., Gimeno, L., and Garcia-Herrera, R.: Trends and extremes of drought indices throughout the 20th century in the Mediterranean, *Nat. Hazards Earth Syst. Sci.*, 11, 33–51, <https://doi.org/10.5194/nhess-11-33-2011>.
- Svoboda, M., LeComte, D., Hayes, M., Heim, R., Gleason, K., Angel, J., Rippey, B., Tinker, R., Palecki, M., Stooksbury, D., Miskus, D., and Stephens, S.: The drought monitor, *B. Am. Meteorol. Soc.*, 83, 1181–1190, <https://doi.org/10.1175/1520-0477-83.8.1181>, 2002.
- Teuling, A. J.: hot future for European droughts, *Nat. Clim. Change*, 8, 364–365, <https://doi.org/10.1038/s41558-018-0154-5>, 2018.
- Teuling, A. J., Seneviratne, S. I., Williams, C., and Troch, P. A.: Observed timescales of evapotranspiration response to soil moisture, *Geophys. Res. Lett.*, 33, L23403, <https://doi.org/10.1029/2006GL028178>, 2006.
- Teuling, A. J., Van Loon, A. F., Seneviratne, S. I., Lehner, I., Aubinet, M., Heinesch, B., Bernhofer, C., Grünwald, T., Prasse, H., and Spank, U.: Evapotranspiration amplifies European summer drought, *Geophys. Res. Lett.*, 40, 2071–2075, <https://doi.org/10.1002/grl.50495>, 2013.
- Tigkas, D. and Tsakiris, G.: Early estimation of drought impacts on rainfed wheat yield in Mediterranean climate, *Environmental Processes*, 2, 97–114, <https://doi.org/10.1007/s40710-014-0052-4>, 2015.
- Tramblay, Y., Koutroulis, A., Samaniego, L., Vicente-Serrano, S. M., Volaire, F., Boone, A., and Polcher, J.: Challenges for drought assessment in the Mediterranean region under future climate scenarios, *Earth-Sci. Rev.*, 210, 103348, <https://doi.org/10.1016/j.earscirev.2020.103348>, 2021.
- Turco, M. and Llasat, M. C.: Trends in indices of daily precipitation extremes in Catalonia (NE Spain), 1951–2003, *Nat. Hazards Earth Syst. Sci.*, 11, 3213–3226, <https://doi.org/10.5194/nhess-11-3213-2011>, 2011.
- Ukkola, A. M., Pitman, A. J., Decker, M., De Kauwe, M. G., Abramowitz, G., Kala, J., and Wang, Y.-P.: Modelling evapotranspiration during precipitation deficits: identifying critical processes in a land surface model, *Hydrol. Earth Syst. Sci.*, 20, 2403–2419, <https://doi.org/10.5194/hess-20-2403-2016>, 2016.
- USGS: MOD16A2 v006, USGS [data set], <https://lpdaac.usgs.gov/products/mod16a2v006/>, last access: 18 October 2022.
- Van Der Knijff, J. M., Younis, J., and De Roo, A. P. J.: LISFLOOD: a GIS-based distributed model for river basin scale water balance and flood simulation, *Int. J. Geogr. Inf. Sci.*, 24, 189–212, <https://doi.org/10.1080/13658810802549154>, 2008.
- Van Loon, A. F.: Hydrological drought explained, *WIREs Water*, 2, 359–392, <https://doi.org/10.1002/wat2.1085>, 2015.
- Vicente-Serrano, S. M., González-Hidalgo, J. C., de Luis, M., and Raventós, J.: Drought patterns in the Mediterranean area: the Valencia region (eastern Spain), *Clim. Res.*, 26, 5–15, <https://doi.org/10.3354/cr026005>, 2004.
- Vicente-Serrano, S. M.: Evaluating the Impact of Drought Using Remote Sensing in a Mediterranean, Semi-arid Region, *Nat. Hazards*, 40, 173–208, <https://doi.org/10.1007/s11069-006-0009-7>, 2006.
- Vicente-Serrano, S. M., Azorin-Molina, C., Peña-Gallardo, M., Tomas-Burguera, M., Domínguez-Castro, F., Martín-Hernández, N., Beguería, S., El Kenawy, A., Noguera, I., and García, M.: A high-resolution spatial assessment of the impacts of drought variability on vegetation activity in Spain from 1981 to 2015, *Nat. Hazards Earth Syst. Sci.*, 19, 1189–1213, <https://doi.org/10.5194/nhess-19-1189-2019>, 2019.
- Wagner, W., Blöschl, G., Pampaloni, P., Calvet, J. C., Bizzarri, B., Wigneron, J. P., and Kerr, Y.: Operational readiness of microwave remote sensing of soil moisture for hydrologic applications, *Hydrol. Res.*, 38, 1–20, <https://doi.org/10.2166/nh.2007.029>, 2007.
- Watts, G., Christerson, B. von, Hannaford, J., and Lonsdale, K.: Testing the resilience of water supply systems to long droughts, *J. Hydrol.*, 414–415, 255–267, <https://doi.org/10.1016/j.jhydrol.2011.10.038>, 2012.
- West, H., Quinn, N., and Horswell, M.: Remote sensing for drought monitoring & impact assessment: Progress, past challenges and future opportunities, *Remote Sens. Environ.*, 232, 111291, <https://doi.org/10.1016/j.rse.2019.111291>, 2019.
- Zampieri, M., D’Andrea, F., Vautard, R., Ciais, P., de Noblet-Ducoudré, N., and Yiou, P.: Hot European summers and the role of soil moisture in the propagation of Mediterranean drought, *J. Climate*, 22, 4747–4758, <https://doi.org/10.1175/2009JCLI2568.1>, 2009.